THE JOURNAL OF PHYSICAL CHEMISTRY A

ARTICLE

pubs.acs.org/JPCA

Evolution of Amide Stacking in Larger γ-Peptides: Triamide H-Bonded Cycles

William H. James III,[†,‡] Evan G. Buchanan,[†] Christian W. Müller,[†,§] Jacob C. Dean,[†] Dmytro Kosenkov,[†] Lyudmila V. Slipchenko,[†] Li Guo,[∥,⊥] Andrew G. Reidenbach,[⊥] Samuel H. Gellman,[⊥] and Timothy S. Zwier*[,†]

[†]Department of Chemistry, Purdue University, 560 Oval Drive, West Lafayette, Indiana 47907-2084, United States

[⊥]Department of Chemistry, University of Wisconsin, Madison, Wisconsin 53706, United States

Supporting Information

ABSTRACT: The single-conformation spectroscopy of two model γ-peptides has been studied under jet-cooled conditions in the gas phase. The methyl-capped triamides, Ac-γ^2-hPhe-γ^2-hAla-NHMe and Ac-γ^2-hAla-γ^2-hPhe-NHMe, were probed by resonant two-photon ionization (R2PI) and resonant ion-dip infrared (RIDIR) spectroscopies. Four conformers of Ac-γ^2-hPhe-γ^2-hAla-NHMe and three of Ac-γ^2-hAla-γ^2-hPhe-NHMe were observed and spectroscopically interrogated. On the basis of comparison with the predictions of density functional theory calculations employing a dispersion-corrected functional (ωB97X-D/6-311++G(d,p)), all seven conformers have been assigned to particular conformational families. The preference for formation of nine-membered rings (C9) observed in a previous study [James, W. H., III et al., *J. Am. Chem. Soc.* **2009**, *131*, 14243] of the smaller analog, Ac-γ^2-hPhe-NHMe, carries over to these triamides, with four of the seven conformers forming C9/C9 sequential double-ring structures, and one conformer a C9/C14 bifurcated double ring. The remaining two conformers form C7/C7/C14 H-bonded cycles involving all three amide NH groups, unprecedented in other peptides and peptidomimetics. The amide groups in these structures form a H-bonded triangle with the two trimethylene bridges forming loops above and below the molecule's midsection. The structure is a natural extension of amide stacking, with the two terminal amides blocked from forming the amide tristack by formation of the C14 H-bond. Pair interaction energy decomposition analysis based on the fragment molecular orbital method (FMO-PIEDA) is used to determine the nonbonded contributions to the stabilization of these conformers. Natural bond orbital (NBO) analysis identifies amide stacking with a pair of n $\rightarrow \pi^*$ interactions between the nitrogen lone pairs and π^* orbitals on the carbonyl of the opposing amide groups.

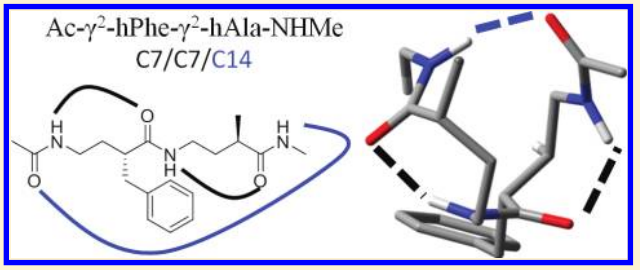

I. INTRODUCTION

Synthetic foldamers that contain amide groups in the backbone have preferred secondary structures that often extend beyond those found in proteins, which are polyamide composed entirely of α-amino acid residues. Principal among such peptide mimics are β-peptides and γ-peptides, which differ from α-peptides by incorporating one and two additional carbon atoms, respectively, between the backbone amide groups.[1] The majority of previous studies have focused attention on β-peptides and mixed α/β-peptides,[2−4] with a variety of constrained and unconstrained substituents incorporated into the β-peptide subunits.

γ-Peptides offer further substituent versatility and added flexibility because of the three-carbon bridge between amide groups, relative to α-peptides (one carbon) or β-peptides (two carbons). Recent progress in the synthesis of γ-amino acids[5−10] is leading to increased effort to understand the folding preferences of γ-peptides.[5,11−18] Though much of this work is aimed at understanding these preferences in the condensed phase, there is a role for studies on small γ-peptide oligomers under isolated conditions, where the inherent preferences can be probed in the absence of solvent effects.[19] Such studies provide a natural point of connection with those testing the ability of molecular mechanics force fields or ab initio methods to properly capture the subtle balance of H-bonding, dispersive forces, and steric strain that lead to the observed conformations.[20−26]

In a recent series of papers, we have explored the conformational preferences and unique spectral signatures of model phenylalanine-containing diamide and triamide β-peptide and α/β-peptide foldamers using single-conformation IR and UV spectroscopy of the jet-cooled molecules.[19,27−30] These studies uncovered a rich array of conformational family types, including single rings varying in size from C5 to C11, sequential double rings (e.g., C8/C7$_{eq}$), and bifurcated double rings (e.g., C5/C8). The "Cn" labeling scheme identifies the number of atoms "n" in the ring closed by an intramolecular NH···O=C H-bond. Diastereomer-specific effects were also explored,[30] as were the

Received: June 13, 2011
Revised: October 6, 2011
Published: October 06, 2011

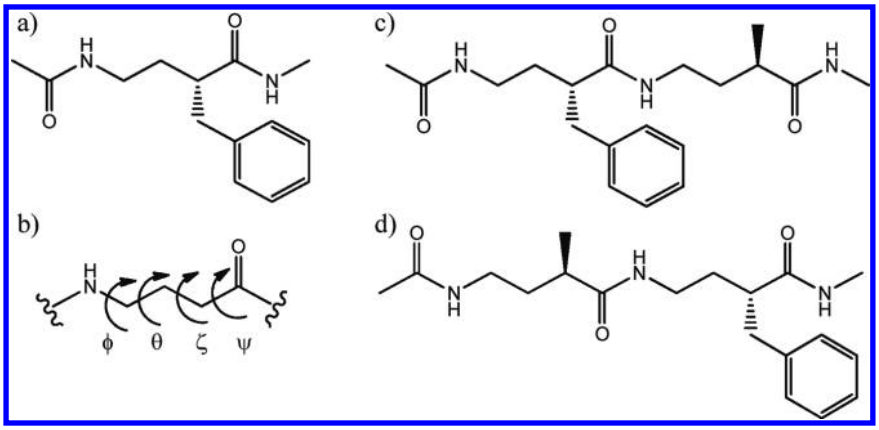

Figure 1. Chemical structures of (a) Ac-γ^2-hPhe-NHMe, (c) Ac-γ^2-hPhe-γ^2-hAla-NHMe, and (d) Ac-γ^2-hAla-γ^2-hPhe-NHMe. (b) Definition of the four dihedral angles present in the γ-peptides.

effects of incorporation of a rigidified residue containing a cyclopentane ring (ACPC) into the β-peptide framework.[29]

Recently, such studies were extended to include a small, capped γ-peptide diamide, Ac-γ^2-hPhe-NHMe (Figure 1a).[19] Here, the presence of a three-carbon spacer provides two additional dihedral angles (θ, ζ) for conformational change beyond the Ramachandran angles (ϕ, ψ) present in α-peptides, as shown in Figure 1b. Under supersonic expansion cooling, this molecule spreads its population over three conformational isomers: two C9 conformers (A(C9(a))) and (B(C9(g−))) and an unusual amide-stacked conformation (C(S(a))). The anti (a), and two gauche positions (g+, g−) refer to the position of the aromatic ring relative to the α carbon. It was a surprising result that a conformation without an intramolecular H-bond could compete with H-bonded conformations for population in the gas phase. This structure was stabilized by a combination of electrostatic and dispersive interactions associated with an antiparallel arrangement of the two amide groups, stacking the amide planes on top of one another much as occurs between stacked aromatic rings.

The presence of an amide stacked conformer in Ac-γ^2-hPhe-NHMe thus afforded the opportunity to characterize this attractive interaction between amide groups, which is likely to be present to some degree in a wide range of other circumstances in which amide groups are brought into close proximity with one another, such as in Asn-Asn and Asn-Gln amide stacks in amyloid-like fibrils.[31] Single-conformation studies were critical to the detection and characterization of amide stacking, enabled by a combination of expansion cooling to trap the population in the zero-point levels of the observed conformers and double-resonance laser spectroscopy to record IR and UV spectra of each conformation free from interference from one another.

That amide stacking is truly competitive with H-bonding was established by mass-resolved infrared population transfer (IRPT) spectra,[19] which determined the abundances of the three conformers of Ac-γ^2-hPhe-NHMe. The amide stacked conformer was shown to comprise 21 ± 1% of the population, approximately half that of the C9 conformers (38 ± 1%, 42 ± 2%). An independent determination under slightly different expansion conditions using both IRPT and its alternative, infrared ion-gain (IRIG) spectroscopy, obtained percentages of 17 ± 1% (IRPT) and 13 ± 5% (IRIG) for the amide stacked conformer (S(a)).[32]

To better understand how amide stacking could compete with H-bonding, a detailed analysis of the nonbonded contributions to the stabilization of the stacked and C9 conformers was carried out using the systematic fragmentation method employing an effective fragment potential (SFM/EFP).[33] This analysis showed that the total nonbonded contributions to stabilization in the amide stacked conformer were about two-thirds as large as that in the C9 H-bonded conformer, with both electrostatic and dispersion forces contributing significantly. In addition, the lack of steric strain in the three-carbon γ-peptide spacer unit produced a turn that brought adjacent amide groups into near-perfect register with one another.

The present work builds naturally upon this previous study by extending single-conformation spectroscopy to larger γ-peptides. Here we probe how the nearest neighbor preferences present in Ac-γ^2-hPhe-NHMe develop in the capped triamides Ac-γ^2-hPhe-γ^2-hAla-NHMe and Ac-γ^2-hAla-γ^2-hPhe-NHMe (Figure 1c,d). The two molecules differ in the ordering of homoalanine and homophenylalanine side chains, serving as direct analogs of the β-peptides Ac-β^3-hPhe-β^3-hAla-NHMe and Ac-β^3-hAla-β^3-hPhe-NHMe studied previously by similar methods.[27,28] We were particularly interested to see whether there is a role for amide stacking in the triamides, or whether the additional possibilities for interamide H-bonds would lead instead only to multiple H-bonded rings. Alternatively, the flexibility of the γ-peptide backbone might lead to structures not yet anticipated, much as occurred in forming amide stacked structures in the diamides.

As we shall see, a total of seven conformers are observed for the two molecules, four of which are assigned as C9/C9 sequential double rings, an extension of the nearest-neighbor preference for C9 rings in the diamide. A fifth structure also makes use of the C9 ring in forming a C9/C14 bifurcated double ring. The remaining two conformers (one for each molecule) show unusual IR spectra that reflect formation of a C7/C7/C14 H-bonded cycle, a H-bonding architecture unprecedented in the other triamides studied to date.[27−30,34−36] Our analysis focuses on understanding the nature and strength of the intramolecular interactions present in this compact, tightly folded structure containing two opposed propylene segment turns and three amide−amide H-bonds.

To complement our experimental studies, we provide an assessment of nonbonded interactions by using pair interaction energy decomposition analysis based on the fragment molecular orbital method (FMO-PIEDA).[37] This scheme provides a way to characterize relative strengths of nonbonded energy components

(electrostatics, polarization, dispersion, exchange-repulsion, and charge transfer) both to the total stability of the conformers and between different parts of the molecule. The factors elucidated include the energetic contributions of individual H-bonds and cooperativity effects. We shall use FMO-PIEDA analysis to gain a deeper understanding of the relative stabilities of the observed conformers, and how they develop in extending the γ-peptide chain from the diamide analog Ac-γ^2-hPhe-NHMe. As we shall see, FMO-PIEDA analysis predicts that a combination of three weaker (more distorted) H-bonds in the C7/C7/C14 H-bonded cycles results in stronger noncovalent interactions than a sum of two stronger H-bonds in C9/C9 sequential double rings. The results also provide a means of understanding the destabilizing effects present in the C9/C14 bifurcated double ring, and the absence of a purely amide stacked structure.

Finally, recent work by Raines and co-workers has highlighted the stabilizing role played by C═O···C═O interactions between amide groups, ascribed via natural bond orbital (NBO) analysis to an n$-\pi^*$ interaction in which the lone pair orbitals on the oxygen of one C═O group overlaps with the π^* orbital of another amide C═O group.[38,39] We carry out an NBO analysis on the C7/C7/C14 triamides and compare it to the corresponding calculations on the amide stacked conformer of Ac-γ^2-hPhe-NHMe. The results point to the stabilizing effect of another type of n$-\pi^*$ interaction in all three, here between the same lone pair orbitals on the amide nitrogen atoms and the π^* orbital on the opposing C═O groups.

II. METHODS

A. Experimental Methods. The synthesis of Ac-γ^2-hPhe-γ^2-hAla-NHMe and Ac-γ^2-hAla-γ^2-hPhe-NHMe was carried out at the University of Wisconsin—Madison on the basis of methodology previously reported for synthesis of γ^2-amino acids and their derivatives.[6] Details on the synthetic route to these triamides are provided in the Supporting Information.

The experimental methods used to carry out the spectroscopic measurements have been described in detail elsewhere.[30,40] Briefly, solid samples of the two γ-peptides were wrapped in glass wool and placed in a glass insert in an effort to reduce thermal decomposition, then inserted into a stainless steel sample holder and heated to approximately 220 °C to increase the sample vapor pressure. The sample holder was located directly behind a pulsed valve (Parker General Valve, Series 9), fitted with a 400 μm diameter nozzle orifice, also heated to this temperature. For the spectroscopic measurements the sample was entrained in a carrier gas of pure neon with a backing pressure of 1.5 bar and expanded into vacuum. The sample molecules were collisionally cooled through collisions with the carrier gas and skimmed prior to entering the ionization region of a time-of-flight-mass-spectrometer (TOF). Low total gas flow rates (2−4 (bar·cm^3)/min) were utilized to minimize interference of the gas pulse with the conical skimmer.

Resonant two-photon ionization (R2PI) spectroscopy was used to record the electronic spectra of the isolated γ-peptide molecules in the S_0-S_1 origin region of the phenylalanine chromophore. The molecules were excited and subsequently ionized with the frequency doubled output of a Nd:YAG pumped tunable dye laser. Typical ultraviolet laser powers used were 0.1−0.5 mJ/pulse. The ultraviolet light traversed the ionization region of the TOF as a collimated beam of approximately 1 mm diameter. The resultant ions were detected by a microchannel plate detector (Jordan TOF, 2.5 cm) fixed atop a one meter long flight tube.

Conformation-specific infrared spectra were recorded using the double resonance method of resonant ion-dip infrared (RIDIR) spectroscopy.[41−43] Tunable infrared radiation in the amide NH stretch spectral region, 3200−3500 cm^{-1}, was obtained using a seeded, Nd:YAG pumped infrared parametric converter (LaserVision). Infrared laser powers in the amide NH stretch region were 3−5 mJ/pulse.

To carry out the RIDIR experiments, the IR (10 Hz) beam counter-propagated the molecular beam, while the UV probe (20 Hz) laser crossed the molecular beam in the ionization region of the TOF-MS.[19] By selection of a delay between IR and UV laser pulses of ∼20 μs, the molecules interrogated by the UV laser were excited as they pass through the skimmer. In this way, all molecules entering the ion source region were exposed to the IR radiation, producing large depletions and removing the need for spatial overlap of the IR and UV beams. With the UV laser wavelength fixed on a particular transition due to a single conformer, the difference in ion signal produced by successive UV laser pulses (one with and one without the IR laser present) was monitored while the IR laser was tuned through the amide NH stretch spectral region. When the IR laser was resonant with a vibrational transition arising from the same ground state as that being probed by the UV laser, depletion in the ion signal was observed. The IR spectrum was recorded by monitoring the output of a gated integrator (Stanford Research Systems) operating in active baseline subtraction mode. The RIDIR absorptions are thus recorded as fractional depletions of the ion signal.

B. Computational Methods. To identify the low-lying minima of Ac-γ^2-hPhe-γ^2-hAla-NHMe and Ac-γ^2-hAla-γ^2-hPhe-NHMe, searches of conformational space were carried out using molecular mechanics force fields (Amber[44] and MMFFs[45]) within the MACROMODEL (Schrödinger) suite.[46] Approximately 200 structures were found for both molecules per search within 50 kJ/mol of the global minimum. All structures within the first 25 kJ/mol (∼200 in total per molecule) were used as input structures for full geometry optimizations at the DFT B3LYP/6-31+G(d) level of theory[47,48] using Gaussian 09 (Rev. A.02).[49] The resultant B3LYP-optimized structures were screened using a 20 kJ/mol energy filter. The remaining conformers (∼50) were submitted for full geometry optimization using the M05-2X dispersion-corrected functional (M05-2X/6-311++G(d,p)) level of theory.[50−52] Harmonic vibrational frequencies and infrared intensities were also calculated at this level of theory.

The calculated spectra were compared with the single-conformation IR spectra. Those structures having both low energy and small standard deviations in wavenumber positions with one of the experimental infrared spectra were submitted to additional DFT calculations at the M06-2X/6-311++G(d,p)[53,54] and ωB97X-D/6-311++G(d,p)[55] levels of theory. The M06-2X calculations employ a newer dispersion parametrized functional developed by the Truhlar group,[44,45] whereas ωB97X-D is a dispersion corrected version of the B97 density functional developed by Head-Gordon and co-workers[55] to include asymptotically correct long-range and dispersive interactions.

For the current work, final assignments were made at the DFT ωB97X-D/6-311++G(d,p) level of theory. Excluding the initial B3LYP optimizations, all DFT calculations employed the keywords scf=tight and int(grid=ultrafine). In arriving at final assignments for the observed conformers, primary consideration was given to the goodness of fit of the calculated NH stretch IR spectra with experiment. This leads to firm assignment to a conformational family, and in most cases a specific structure. Free

energy calculations for each conformer were calculated at the pre-expansion temperature (493 K) to provide a prediction of the population of each conformer prior to jet-cooling.

As an additional point of comparison between experiment and theory, single-point TDDFT calculations[56,57] were carried out at the M05-2X, M06-2X, and ωB97X-D levels of theory to provide predictions for the relative wavelengths of the S_0-S_1 electronic transitions of the conformers, with the ωB97X-D/6-311++G(d,p) calculations reported in the text. These calculations play, at best, a confirmatory role.

Pair interaction energy decomposition analysis based on the fragment molecular orbital method (FMO-PIEDA) was performed to characterize the nonbonded interactions in the triamides. FMO[58,59] is a fragmentation technique in which a molecule is divided into fragments and the electron density of each fragment is optimized in a Coulomb bath of the other fragments. Separation of a molecule into fragments makes it possible to evaluate the interaction energies between fragments leading to an energy decomposition analysis. In the present work, the latter is realized using the PIEDA approach. The MP2/6-31G* level of theory[60] was employed in FMO calculations. A choice of this relatively small basis set is justified by the best agreement of the MP2 total relative energies of conformers with the ωB97X-D/6-311++G(d,p) results, with discrepancies not exceeding 3 kJ/mol. Additionally, larger basis sets are known to result in instabilities in FMO and energy decomposition analysis due to increasing charge transfer effects.[61,62]

To evaluate noncovalent interactions, we split the triamides into three fragments at the γ^2 C−N bonds, e.g., $CH_3-CO-NH-$, $-C(CH_2-C_6H_5)-CO-NH-$, and $-C(CH_3)-CO-NH-CH_3$ for Ac-γ^2-hPhe-γ^2-hAla-NHMe, and capped these fragments with hydrogens. FMO-PIEDA calculations were performed for the resulting trimers held in configurations corresponding to the seven assigned triamide conformers. For noncovalent systems, FMO-PIEDA analysis is almost exactly analogous to the Kitaura−Morokuma energy decomposition scheme,[63] apart from small differences in charge transfer and exchange components due to three-body and higher-order terms, with dispersion interactions included through the MP2 correlation energy. The FMO-PIEDA analysis performed in this work can be compared with the SFM/EFP[64,65] energy decomposition employed for Ac-γ^2-hPhe-NHMe in our previous study.[19] In SFM/EFP, the amides were fragmented into smaller groups ($-CO-NH-$, $-CH_2-$, CH_3-) and capped with hydrogens. The noncovalent interactions between different groups were evaluated using the effective fragment potential method.[64,65] The FMO-PIEDA scheme used in the current work employs larger fragments ($CH_3-CO-NH-$ and $-CH(CH_2-C_6H_5)-CO-NH-CH_3$). We have found that the use of larger fragments ensures better preservation of partial charges and polarization of the original gamma-peptides and creates fewer artifacts.

Finally, natural bond orbital (NBO) analysis[66] was carried out on the structures obtained by the ωB97X-D calculations to view the interactions present in the assigned conformational isomers from this vantage point, for comparison with the corresponding analysis of amide−amide interactions by Raines and co-workers.[38,39]

III. RESULTS

A. R2PI and RIDIR Spectra. Figure 2a presents the R2PI spectrum of Ac-γ^2-hPhe-γ^2-hAla-NHMe in the S_0-S_1 region of the phenylalanine side chain (37 400−37 750 cm^{-1}). The spectrum shows four dominant transitions between 37 500 and 37 600 cm^{-1}, and several weaker transitions spread throughout the spectral region. As we shall soon see, the labeled transitions arise from unique conformational isomers, appearing at 37 535 (A), 37 511 (B), 37 542 (C), and 37 600 cm^{-1} (D). The spectra are in the same wavelength region as in Ac-γ^2-hPhe-NHMe (Table 1), where the two C9 conformers had S_0-S_1 origin transitions at 37 484 and 37 585 cm^{-1}, and the stacked conformation at 37 471 cm^{-1}. Furthermore, each conformer of Ac-γ^2-hPhe-γ^2-hAla-NHMe shows only weak low-frequency vibronic activity, suggesting only weak interactions of the aromatic ring in these conformers with the γ-peptide backbone.

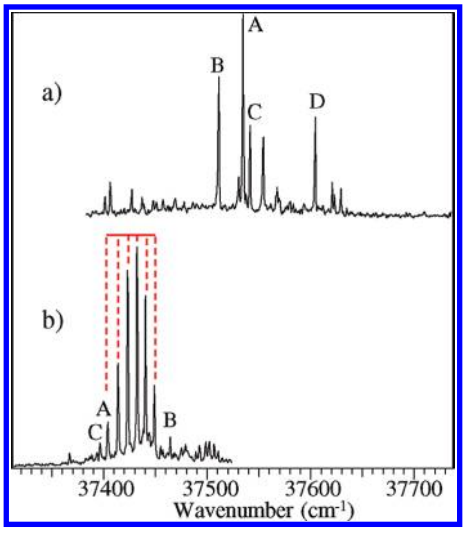

Figure 2. Resonant two-photon ionization spectra in the S_0-S_1 origin region of (a) Ac-γ^2-hPhe-γ^2-hAla-NHMe and (b) Ac-γ^2-hAla-γ^2-hPhe-NHMe. The progression marked in tie lines belongs to conformer A. Scans over a wider wavelength range showed no additional transitions over the 37 250−37 750 cm^{-1} region.

In notable contrast, the vast majority of the vibronic structure present in the R2PI spectrum of Ac-γ^2-hAla-γ^2-hPhe-NHMe (Figure 2b) is due to a single conformer, labeled A (37 404 cm^{-1}), which exhibits a long and intense Franck−Condon progression in a mode with a 9 cm^{-1} vibrational frequency. Two other transitions with sizable intensity, B (37 464 cm^{-1}) and C (37 396 cm^{-1}) have much weaker low-frequency vibronic activity. All three transitions are shifted to lower wavenumber than any found in Ac-γ^2-hPhe-NHMe or Ac-γ^2-hPhe-γ^2-hAla-NHMe, reflecting possible differences, perhaps substantial ones, in the environment about the phenyl ring.

To gain further insight into the conformational preferences of Ac-γ^2-hPhe-γ^2-hAla-NHMe and Ac-γ^2-hAla-γ^2-hPhe-NHMe, single-conformation infrared spectra of each of the labeled transitions in Figure 2 were recorded in the amide NH spectral region (3300−3500 cm^{-1}). The spectra for the four conformers of Ac-γ^2-hPhe-γ^2-hAla-NHMe (Figure 3A−D) each show three NH stretch transitions due to the three amide NH groups in the triamides. It is immediately evident from the spectra that there are two distinct conformational families present in Ac-γ^2-hPhe-γ^2-hAla-NHMe. The spectra of conformers A, B, and D show a close similarity, whereas that of conformer C is unique. The spectra of conformers A, B, and D have two broadened, intense transitions below 3350 cm^{-1} due to H-bonded NH groups and a sharp single transition near 3480 cm^{-1} ascribable to a free amide NH

Table 1. Spectroscopic Data Recorded and Conformational Assignments for Ac-γ^2-hPhe-NHMe, Ac-γ^2-hPhe-γ^2-hAla-NHMe, and Ac-γ^2-hAla-γ^2-hPhe-NHMe

conformer	H-bond family	specific structure	expt S_0-S_1 (cm^{-1})	expt amide NH stretches (cm^{-1})[a]		
			Ac-γ^2-hPhe-NHMe			
A	C9	C9(a)	37 584		3372	3481
B	C9	C9(g-)	37 484		3357	3474
C	Amide Stacked	S(a)	37 471		3469	3480
			Ac-γ^2-hPhe-γ^2-hAla-NHMe			
A	C9/C9	C9/C9(a)	37 535	3331	3339	3482
B	C9/C9	C9/C9(g-)	37 511	3313	3327	3477
C	C7/C7/C14	C7/C7/C14(g-)	37 542	3341	3391	3397
D	C9/C9	C9/C9(g+)	37 600	3324	3336	3482
			Ac-γ^2-hAla-γ^2-hPhe-NHMe			
A	C9/C9	C9/C9(a)	37 404	3302	3313	3480
B	C9/C14	C9/C14(a)	37 464	3394	3436	3482
C	C7/C7/C14	C7/C7/C14(g-)	37 396	3349	3393	3399

[a] The 3417 cm transition in conformer A and 3412/3420 cm transitions in conformer B of Ac-γ^2-hAla-γ^2-hPhe-NHMe are Fermi resonances from amide I overtones.

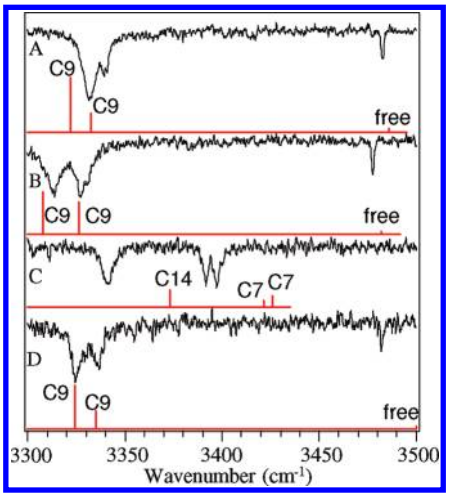

Figure 3. Resonant ion-dip infrared spectra of the resolved conformers of Ac-γ^2-hPhe-γ^2-hAla-NHMe in the amide NH stretch spectral region (black traces) and ωB97X-D/6-311++G(d,p) scaled (0.9466) harmonic vibrational frequencies and infrared intensities (red traces, as sticks).

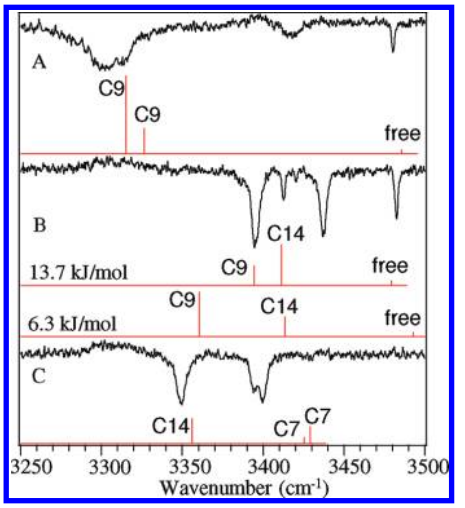

Figure 4. Resonant ion-dip infrared spectra of the resolved conformers of Ac-γ^2-hAla-γ^2-hPhe-NHMe in the amide NH stretch spectral region (black traces) and ωB97X-D/6-311++G(d,p) scaled (0.9466) harmonic vibrational frequencies and infrared intensities (red traces, as sticks). The two stick spectra beneath experimental spectrum B represent the two best-fit C9/C14(a) calculated spectra.

(Table 1). The location of the H-bonded transitions in conformers A, B, and D is near that of the single-ring C9 H-bonds of Ac-γ^2-hPhe-NHMe,[19] which were found at 3357 and 3372 cm^{-1}. On this basis, the three conformers A, B, and D are tentatively assigned as C9/C9 sequential double ring structures.

The infrared spectrum of conformer C is striking in that all three of its NH stretch fundamentals are shifted below 3400 cm^{-1} and are broadened, providing strong evidence that all three NH groups are involved in H-bonds. The triad of peaks is composed of a single band at 3341 cm^{-1}, and a closely spaced doublet at 3391 and 3397 cm^{-1}. This is an unprecedented result, in that there is no previous example in other capped triamides studied to date (α-, α/β-, and β-peptides) in which three intramolecular H-bonds are formed. This is a testimony again to the unusual flexibility of the γ-peptides the same characteristic that produced amide stacking in the diamide analog Ac-γ^2-hPhe-NHMe.[19]

The corresponding IR spectra of the three conformers of Ac-γ^2-hAla-γ^2-hPhe-NHMe are shown in Figure 4A–C. Of the three, only that of conformer Ac-γ^2-hAla-γ^2-hPhe-NHMe (C) bears an immediate resemblance to one already observed in Ac-γ^2-hPhe-γ^2-hAla-NHMe, in that case Ac-γ^2-hPhe-γ^2-hAla-NHMe (C), possessing three amide–amide H-bonds. The unique aspects of the spectra of conformers A and B (Figure 4A, B) make assignment difficult without the assistance of calculations (as taken up in the next section). However, certain aspects are worth noting immediately.

The spectrum of conformer A has a sharp transition at 3480 cm^{-1}, which is clearly assigned to a free amide NH stretch. The peak at 3302 cm^{-1} is unusually broad and has a shoulder at 3312 cm^{-1}, suggesting the presence of two bands in this region.

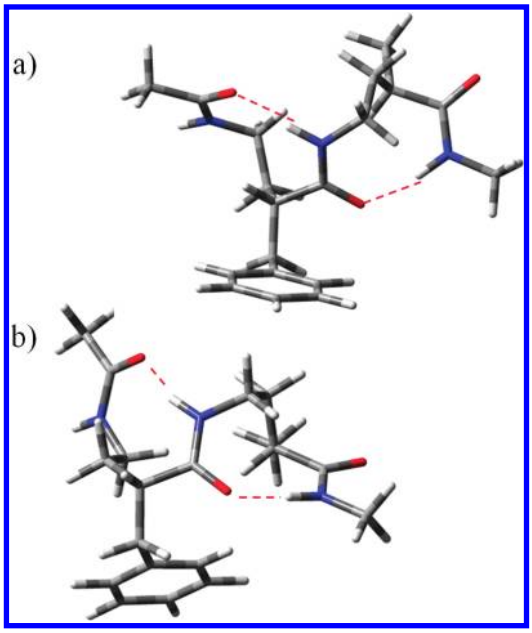

Figure 5. Optimized structures for (a) the C9/C9(a) structure assigned to conformer A and (b) C9/C9(g+) assigned to conformer D of Ac-γ^2-hPhe-γ^2-hAla-NHMe. The structures for conformation B of Ac-γ^2-hPhe-γ^2-hAla-NHMe and conformation A of Ac-γ^2-hAla-γ^2-hPhe-NHMe differ from that in (a) in the position of the aromatic ring. See text for further discussion.

The weak, broadened transition appearing at 3418 cm^{-1} could be a weakly bound NH (e.g., an NH$\cdots\pi$), but this would constitute a fourth transition if the band near 3300 cm^{-1} is indeed a doublet. Alternatively, the band at 3418 cm^{-1} could be an amide I (primarily C═O stretch) overtone (2 × 1709 cm^{-1}).

The spectrum of conformer B has three strong transitions at 3394, 3436, and 3482 cm^{-1} that are almost certainly due to the three amide NH stretch fundamentals. Weak transitions at 3412 and 3420 cm^{-1} are either combination bands or amide I overtones. The lowest frequency band is clearly involved in an intramolecular H-bond, whereas the band at 3436 cm^{-1} may reflect the presence of a weak H-bond with another amide group or the phenyl ring.

B. Comparison with Calculations. As stated in the Experimental Methods (section II.A), structural optimizations and vibrational frequency calculations for the low-lying conformers of Ac-γ^2-hPhe-γ^2-hAla-NHMe and Ac-γ^2-hAla-γ^2-hPhe-NHMe were carried out using DFT M05-2X, M06-2X, and ωB97x-D functionals with a 6-311++G(d,p) basis set. For the remainder of this paper we will focus our attention on the results of the ωB97X-D calculations; however, M05-2X and M06-2X calculations with the same basis set lead to identical assignments. The results (relative energies, scaled vibrational frequencies, infrared intensities, and single-point electronic excitation energies) for the conformations of interest using these density functionals can be found in the Supporting Information.

1. Ac-γ^2-hPhe-γ^2-hAla-NHMe. The four conformers of Ac-γ^2-hPhe-γ^2-hAla-NHMe have been divided into two families by inspection of the single-conformation infrared spectra. The tentative assignment of conformers A, B, and D as C9/C9 sequential double rings is confirmed and strengthened by the calculations, which predict the presence of several C9/C9 sequential double ring structures among the lowest energy structures.

The stick diagrams immediately below the experimental spectra show the calculated vibrational frequencies (scaled by 0.9466) and infrared intensities at the ωB97X-D/6-311++G(d,p) level of theory for the C9/C9 structures that best reproduce the experimental spectra of conformers A, B, and D. The match between experiment and theory, in terms of both frequencies and relative intensities, is quite good. The C9/C9 double rings characteristically have two C9 NH stretch fundamentals close in frequency, with relative intensities dictated by the degree of coupling between them.

Two of the three C9/C9 structures of Ac-γ^2-hPhe-γ^2-hAla-NHMe (A and D) share identical C9/C9 backbones (shown in Figure 5a), differing only in the position of the phenylalanine side chain, anti, or gauche+ (abbreviated as a, g+).[19,27−30] One of the two C9 rings in conformer D has a different set of dihedral angles (C9b, Table 3). Their relative zero-point corrected energies and free energies calculated at the pre-expansion nozzle temperature (493 K) are listed in Table 2. The C9/C9(g−) structure assigned to B is calculated to be the global minimum, whereas that assigned to A (C9/C9(a)) is only 1.6 kJ/mol above it. This energy ordering is retained when free energies are considered (Table 2). The structure assigned to conformer D (C9/C9(g+)) is 8.3 kJ/mol above B in internal energy but drops to within 2 kJ/mol of the global minimum in relative free energy, presumably due to differences in its vibrational frequencies associated with incorporation of the C9b ring and the g− phenyl ring position.

Because the structure responsible for the infrared spectrum of conformer C must possess three amide−amide H-bonds, the search of conformational space quickly reduced to members of a single conformational family, labeled as C7/C7/C14, with all other potential triply H-bonded structural motifs sterically forbidden. The calculated infrared spectrum shown in Figure 3C is that of the lowest energy C7/C7/C14 conformer, C7/C7/C14-(g−), with a relative energy (free energy) of 1.5 (1.9) kJ/mol. This structure (shown in Figure 6a) is a H-bonded cycle in which all three amide groups act simultaneously as donor and acceptor via sequential C7 rings closed by a C14 cycle between terminal groups. Whereas the calculated spectrum has the right pattern, the vibrational frequencies obtained using the scale factor that matched so well for the C9/C9 structures (0.9466) predict frequencies that are systematically too high by ∼30 cm^{-1}. We will return to consider this structure and its challenge for theory in the Discussion but merely note here that all levels of theory suffered from the same deficiency, with the results of ωB97x-D calculations closest to experiment.

2. Ac-γ^2-hAla-γ^2-hPhe-NHMe. The stick spectra in Figure 4 are those predicted by calculation as best matches with experiment for the three conformers of Ac-γ^2-hAla-γ^2-hPhe-NHMe. As anticipated on the basis of its similarity to Ac-γ^2-hPhe-γ^2-hAla-NHMe (C), Ac-γ^2-hAla-γ^2-hPhe-NHMe (C) is also a C7/C7/C14 H-bonded cycle with peptide backbone structure identical to that in Ac-γ^2-hPhe-γ^2-hAla-NHMe (C) (Figure 6b), with all three NH groups involved in H-bonds. There are two C7/C7/C14 conformers that are potential candidates: C7/C7/C14(g−) with a calculated relative energy only 0.3 kJ/mol above the global minimum and C7/C7/C14(a), for which E_{rel} = 0.6 kJ/mol. The calculated free energies for these two structures are 4.3 and 1.1 kJ/mol, respectively. The calculated IR spectrum (Figure 4C) for the (g−) conformer is a somewhat better match with experiment, and without strong energetic preferences between the two, we tentatively assign the observed conformer on that basis as C7/C7/C14(g−).

Table 2. Calculated Data at the DFT ωB97X-D/6-311++G(d,p) Level of Theory

conformer	H-bond family	structure	ΔE (kJ/mol)	ΔG^{493} (kJ/mol)	TDDFT S_0-S_1 (cm-1)[a]	calc amide NH stretches (cm^{-1})[b]		
			Ac-γ^2-hPhe-γ^2-hAla-NHMe					
A	C9/C9	C9/C9(a)	1.59	0.52	37 535	3322	3333	3486
B	C9/C9	C9/C9(g-)	0.00	0.00	37 440	3308	3326	3482
C	C7/C7/C14	C7/C7/C14(g-)	1.49	1.94	37 443	3373	3422	3426
D	C9/C9	C9/C9(g+)	8.31	2.20	37 248	3324	3335	3500
			Ac-γ^2-hAla-γ^2-hPhe-NHMe					
A	C9/C9	C9/C9(a)	3.24	0.71	37 404	3315	3326	3485
B	C9/C14	C9/C14(a)	13.75	0.00	37 501	3394	3411	3479
C	C7/C7/C14	C7/C7/C14(g-)	0.32	4.28	37 393	3356	3425	3429

[a] Scaled 0.8562 for Ac-γ^2-hPhe-γ^2-hAla-NHMe and 0.8563 for Ac-γ^2-hAla-γ^2-hPhe-NHMe single point TDDFT ωB97X-D/6-311++G(d,p). [b] Scaled 0.9466 ωB97X-D/6-311++G(d,p).

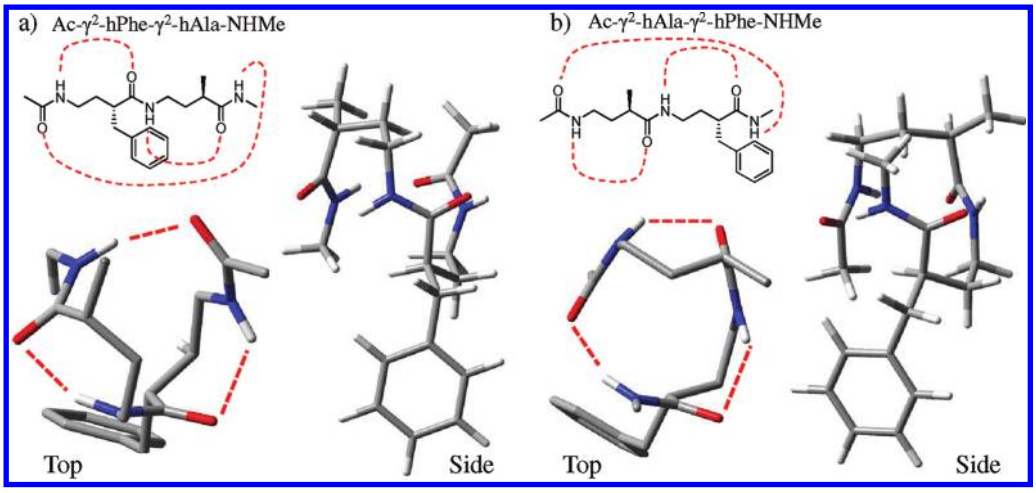

Figure 6. C7/C7/C14(g-) structures assigned to conformer C of (a) Ac-γ^2-hPhe-γ^2-hAla-NHMe and (b) Ac-γ^2-hAla-γ^2-hPhe-NHMe. The chemical structures in each show the C14 and two C7 H-bonds. The structures viewed from the top have most of the H-atoms removed for clarity.

As already discussed in section III.A, the IR spectrum of conformer A (Figure 4A) could not be assigned with certainty on the basis of its pattern alone. After careful searches of possibilities, the spectrum is assigned as a C9/C9 double-ring structure (C9/C9(a), Figure 5b) with a relative energy of 3.2 kJ/mol. The calculated spectrum faithfully reproduces the close-lying pair of H-bonded NH stretch bands near 3300 cm^{-1} characteristic of the C9/C9 double-ring, which are only partially resolved in the experimental spectrum, appearing at 3331 and 3339 cm^{-1}.

This assignment associates the transition at 3418 cm^{-1} with overtones/combination bands of amide I vibrations. Without experimental spectra in the amide I region, a firm assignment is not possible; however, this band is in the right region on the basis of the frequencies of the C9 and free amide C═O stretch fundamentals in Ac-γ^2-hPhe-NHMe (1693 and 1710 cm^{-1}, respectively).

The ultraviolet spectrum provides confirming evidence for this assignment. Recall that this conformer has a long Franck–Condon progression involving an unusually low-frequency vibrational mode (9 cm^{-1}). Of the possible structures, C9/C9(a) has a calculated lowest-frequency vibration of 14 cm^{-1}, whereas other conformers are above 20 cm^{-1}. Furthermore, the form of this vibration, included in the Supporting Information, shows substantial motion of the entire N-terminal portion of the γ-peptide chain relative to the phenylalanine side chain, with the γ^4 carbon in close proximity to the ring (3.6 Å). We propose that $\pi-\pi^*$ excitation of the phenyl ring produces a geometry change along this normal mode, producing the long Franck–Condon progression.

The unique IR spectrum of Ac-γ^2-hAla-γ^2-hPhe-NHMe (B) (Figure 4B) is best fit as a C9/C14 bifurcated double ring structure, with two possibilities shown (Figure 7). The match between experiment and theory is not of the same quality as in other conformers; however, this may be a consequence of the bifurcated structure in which two NH groups H-bond to the same C═O group. A major consequence of this type of interaction is the much smaller shift of both NH fundamentals, with the calculations also predicting strong coupling between them. The calculations do not seem to capture either the frequency shift or the interamide coupling with quantitative accuracy in this case. As with conformer A, the weak transitions near 3415 cm^{-1} are tentatively assigned to amide I overtones, although a minor contribution from a fourth conformer cannot be ruled out entirely. The calculations predict conformer B as the global free energy minimum, due to the larger number of low frequency vibrations associated with the C9/C14 structure (Table 3) that lower its free energy relative to the other conformers.

3. S_0-S_1 Electronic Frequency Shifts. The single-conformation IR spectra have provided firm assignments to conformational families for all seven observed conformers of the two

molecules. The R2PI spectra also provide the wavenumber positions of the S_0-S_1 electronic origins, which can also be compared with calculation. Such a comparison not only tests the calculations but also can provide a final point of distinction between alternative assignments to particular structures within a given conformational family. On the basis of the size of the molecules, full excited state optimizations were not carried out. Instead, single-point TDDFT vertical excitation energies at the DFT ωB97X-D/6-311++G(d,p) level of theory were calculated. In all but one case (Ac-γ^2-hAla-γ^2-hPhe-NHMe (A)), the experimental R2PI spectra have S_0-S_1 origins that are dominated by the electronic origins, making the comparison of experiment with vertical excitation energies reasonable.

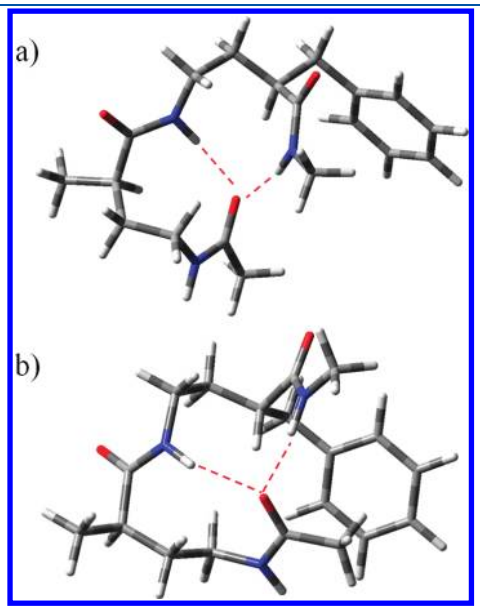

Figure 7. Two possible C9/C14 bifurcated double ring structures for conformer B of Ac-γ^2-hAla-γ^2-hPhe-NHMe: (a) C9/C14(a) and (b) C9/C14(a)′.

Table 2 summarizes the calculated vertical excitation energies for the S_0-S_1 excitations of the conformers. A single scale factor (0.8562) was established by choosing it so as to match the experimental S_0-S_1 origin (37 535 cm^{-1}) and calculated vertical excitation energies for conformer A of Ac-γ^2-hPhe-γ^2-hAla-NHMe (43 840 cm^{-1}). The calculations capture the observed shift to the red by about 130 cm^{-1} of the electronic origins of Ac-γ^2-hAla-γ^2-hPhe-NHMe relative to Ac-γ^2-hPhe-γ^2-hAla-NHMe. Furthermore, they also faithfully reproduce the relative positions of the S_0-S_1 origins of the three conformers of Ac-γ^2-hAla-γ^2-hPhe-NHMe. In fact, the vertical TDDFT results provide evidence that Ac-γ^2-hAla-γ^2-hPhe-NHMe (B) is C9/C14(a) rather than C9/C14(g−) on the basis of the calculated shifts for the two structures. A similar preference for the assignment of Ac-γ^2-hAla-γ^2-hPhe-NHMe (C) as C7/C7/C14(g−) over C7/C7/C14(a) can be made on the basis of the TDDFT results (Table 2).

The comparison of experimental and calculated electronic frequency shifts in Ac-γ^2-hPhe-γ^2-hAla-NHMe is less satisfactory, however. In particular, whereas the relative positions of conformers A and B are reproduced by calculation, the calculated electronic frequency shifts for C and D are in the opposite direction (red shift of −92 and −287 cm^{-1}) relative to experiment (+7 and +65 cm^{-1}). The assigned structure for conformer D (Figure 5b) has a close interaction of a backbone CH_2 group with the phenyl ring. On the basis of frequency shifts in other phenyl derivatives, one would anticipate a small red shift on this basis. A possible explanation for the discrepancy is that the calculations overestimate the magnitude of this interaction. Alternatively, the R2PI spectrum does contain weak transitions further to the red (Figure 1a), one of which could be the actual

Table 3. Calculated Peptide Backbone Dihedral Angles at the DFT ωB97X-D/6-311++G(d,p) Level of Theory for Ac-γ^2-hPhe-NHMe, Ac-γ^2-hPhe-γ^2-hAla-NHMe, and Ac-γ^2-hAla-γ^2-hPhe-NHMe[a]

conformer	specific structure	peptide backbone dihedral angles (φ, θ, ζ, ψ)	
		Ac-γ^2-hPhe-NHMe	
A	C9(a)	(+99, −70, −73, +105)	
B	C9(g−)	(+98, −67, −78, +99)	
C	S(a)	(−102, +55, −76, +136)	
*[b]	S′(a)	(+71, +61, −62, −66)	
*	C7(a)	(−176, −63, +92, +136)	
		Ac-γ^2-hPhe-γ^2-hAla-NHMe	
A	C9/C9(a)	(+98, −70, −72, +100)	(+96, −68, −75, +95)
B	C9/C9(g−)	(+97, −68, −76, +96)	(+96, −67, −75, +94)
C	C7/C7/C14(g−)	(−158, +75, −61, +139)	(+81, +73, −52, −90)
D	C9b/C9(g+)	(+72, −157, +53, +26)	(+98 −63, −78, +90)
		Ac-γ^2-hAla-γ^2-hPhe-NHMe	
A	C9/C9(a)	(+98, −69, −72, +100)	(+99,-66, −75, +95)
B[c]	C9/C14(a)	(+99, −71, −74, +102)	(−159, −61, −55, +113)
	C9/C14(a)′	(−69, +162, −58, −31)	(−78, −63, −74, +108)
C	C7/C7/C14(g−)	(+85, +60, −66, −78)	(−148, +55, −80, +156)
*	S(a)′/S(a)	(−72, −58, +65, +67)	(−104, +55, −76, +140)
*	S/S(a)	(−101, +57, −77, +141)	(−101, +64, −84, +141)

[a] Definitions of the dihedral angles (ϕ, θ, ζ, ψ) are given in Figure 1. [b] Not observed experimentally [c] Two possible structures for conformer B.

S_0-S_1 origin of conformer D. Further experimental and theoretical work is needed to resolve this issue.

IV. DISCUSSION

A. Conformational Preferences of γ^2-Peptide Triamides Compared to Ac-γ^2-hPhe-NHMe. One of the primary motivations of the present study was to determine and understand how the conformational preferences present in the smallest γ-peptide, Ac-γ^2-hPhe-NHMe, develop as the peptide backbone is extended. Here we have taken the first logical step in studying the triamides Ac-γ^2-hPhe-γ^2-hAla-NHMe and Ac-γ^2-hAla-γ^2-hPhe-NHMe. To facilitate a quantitative comparison between the structures, Table 3 compares the (ϕ, θ, ζ, ψ) dihedral angles of the observed structures, extracted from the calculations, on the basis of the assignments just made.

1. C9-Containing Structures. In Ac-γ^2-hPhe-NHMe, two of the three observed conformers were C9 single-ring structures in which the two amide groups bind together to form a nine-membered intramolecular H-bonded ring.[19] This dominant nearest-neighbor structural motif was present in five of the seven conformers detected in Ac-γ^2-hPhe-γ^2-hAla-NHMe and Ac-γ^2-hAla-γ^2-hPhe-NHMe. Four of these structures (Ac-γ^2-hPhe-γ^2-hAla-NHMe (A,B,D) and Ac-γ^2-hAla-γ^2-hPhe-NHMe (A)) are C9/C9 sequential double rings, and one (Ac-γ^2-hAla-γ^2-hPhe-NHMe (B)) is a C9/C14 bifurcated double ring. With but one exception, the dihedral angles present in the C9 rings ($\phi = +99°$, $\theta = -70°$, $\zeta = -73°$, $\psi = +105°$) were the same as those found in Ac-γ^2-hPhe-NHMe, differing by at most a few degrees (Table 3). In this ring, the two amide planes approach one another at an angle of ~40°, and an H···O distance of only 1.90 Å. We call this ring C9a. In Ac-γ^2-hPhe-γ^2-hAla-NHMe (D), the assigned structure, shown in Figure 5b), has one C9 ring (C9b, N-terminal C═O to interior N—H) with dihedral angles +72°, −157°, +53°, and +26° (Table 3). In this case, the C9 ring is more nearly flat, with the two amide groups close to coplanar (~15°) with an H···O distance of 1.97 Å.

One of the notable aspects of the IR spectra of small peptides is the insights they provide to cooperative effects in H-bonds.[30] Sequential double rings form by having the interior amide group involved in both H-bonded rings, with the NH group serving as H-bond donor in one and the C═O as acceptor in another. The NH stretch IR spectra of the C9/C9 sequential double rings (Figure 3A,B,D and Figure 4A) have NH stretch fundamentals due to the two H-bonded NH groups appearing near 3300 cm^{-1}, approximately 30 cm^{-1} lower in frequency than in the C9 single ring structures found in Ac-γ^2-hPhe-NHMe.[19] This indicates a strengthening of the H-bonds in the double ring, which is reflected structurally in a slight shortening of the NH···O distance from 1.95 Å to 1.88−1.92 Å in the C9/C9 structures. In addition, the two NH stretch modes in the C9/C9 double rings are coupled to one another, appearing as symmetric and antisymmetric combinations, leading to an asymmetry in the two IR intensities reflecting a partial cancellation of dipole derivatives in one case, and enhancement in the other.

It is informative to compare the dihedral angles present in the C9/C9 conformers observed in this work with those present in the repeating units calculated by Baldauf et al. for γ-peptide hexamers.[21] The C9a ring that is pervasive in the conformers we observe is predicted by calculation to be the repeating unit of a low energy helix (H^I_9) at the HF/6-31G* level of theory. The C9b ring, on the other hand, possesses dihedral angles similar to those of the H^{II}_9 helix, although there is some deviation in the final two angles. This deviation is likely the result of additional H-bonding interactions present in the hexamers that are absent in the triamides studied here. Thus, the strong preference for formation of C9a and C9b rings observed in Ac-γ^2-hPhe-γ^2-hAla-NHMe and Ac-γ^2-hAla-γ^2-hPhe-NHMe is predicted to be retained in the secondary structures formed by larger γ-peptide oligomers.

The C9/C14 bifurcated double ring structure assigned to Ac-γ^2-hAla-γ^2-hPhe-NHMe (B) reflects a competition for electron density among the two NH groups H-bonding to the same C═O group, which in turn weakens both interactions. A similar conclusion was reached by Yang et al. in their study of three-center HXH H-bonds.[67] As already noted, this shifts the NH stretch fundamentals to much higher frequency, with NH stretch fundamentals at 3394 and 3436 cm^{-1}, some 60−130 cm^{-1} higher in frequency than the C9/C9 fundamentals. The calculated structures also reflect a weakening of the H-bonds, with a C9 NH···O distance of 2.06 Å, ~0.15 Å longer than in the C9/C9 sequential double rings.

2. C7/C7/C14 H-Bonded Cycles. The identification and characterization of two conformers assigned as C7/C7/C14 H-bonded cycles (Ac-γ^2-hAla-γ^2-hPhe-NHMe (C) and Ac-γ^2-hPhe-γ^2-hAla-NHMe (C)) is arguably the most interesting result of the present study. These C7/C7/C14 cycles are first examples of a triamide cycle in which all three amide groups are involved in H-bonds both as donors and as acceptors in a triangular structure. Interestingly, this structure incorporates two C7 H-bonded rings, despite the fact that no such structure was observed in Ac-γ^2-hPhe-NHMe.[19] Formation of a triply H-bonded cycle is made possible by the flexibility and separation between amide groups inherent to the γ-peptide backbone; no analogous structure is known among α-peptides.

Parts a and b of Figures 6 present two different views of the optimized structures calculated for the two C7/C7/C14 cycles, Ac-γ^2-hPhe-γ^2-hAla-NHMe (C) and Ac-γ^2-hAla-γ^2-hPhe-NHMe (C), respectively. These are fascinating structures, with the amide groups forming H-bonded cycles around the molecule's "waist", with the three-carbon segments forming loops that project above and below the polar amide groups. In one view in Figure 6 the alkyl and aromatic hydrogens have been removed to better expose the H-bonding cycle. Both structures have one loop above the waist and one below, with the two structures differing in which loop is above and which below, as viewed from N-terminus to C-terminus. This changes the orientation of the amide groups with respect to one another.

Two sides of the triangle formed by the three amide groups are connected by weak, highly bent C7 H-bonds between the two terminal amide groups and the interior amide. A C14 H-bond closes the cycle, joining the two terminal amide groups. The calculated NH···O H-bond lengths for the C7 H-bonds are both ~2.15 Å, with acute angles of approach of the involved amide planes. The dihedral angles (Table 3) for the two C7 rings differ in that one forms a chair (with +, +, −, − dihedrals) and the other a boat conformation (with −, +, −, + dihedrals) between the γ^3 carbon and the NH···O═C groups. This is to be contrasted with the γ-C7 single-ring structures, in which the two amide groups are nearly in-plane with one another, with an NH···O distance of 1.90 Å. Thus, the two C7 rings are far from optimal but are uniquely capable of also forming a third C14 H-bond that closes the cycle.

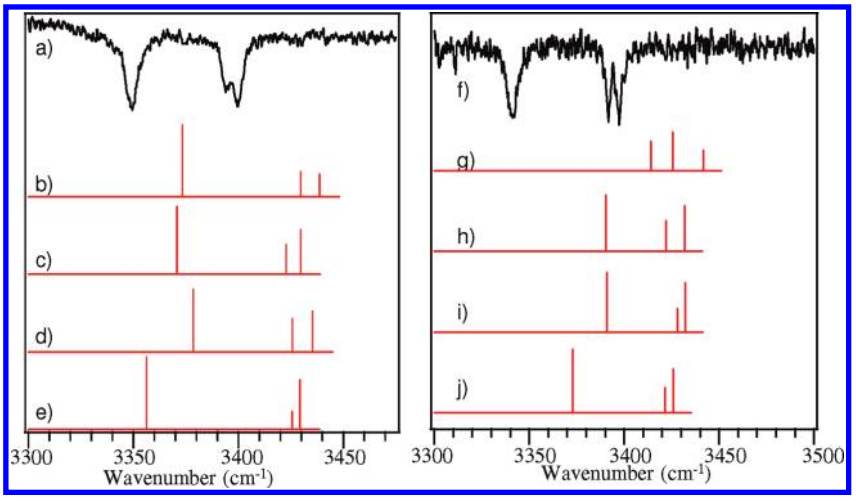

Figure 8. RIDIR spectrum of the conformer C of (a) Ac-γ^2-hAla-γ^2-hPhe-NHMe C7/C7/C14(g-) and (b) conformer C of Ac-γ^2-hPhe-γ^2-hAla-NHMe C7/C7/C14(g-) compared to the predictions at the (b, g) DFT B3LYP/6-31+G(d) (scaled 0.9600), (c, h) M05-2X/6-311++G(d,p) (scaled 0.9417), (d, i) M06-2X/6-311++G(d,p) (scaled 0.9489), and (e, j) ωB97X-D/6-311++G(d,p) (scaled 0.9466) levels of theory.

In contrast, the C14 H-bond is much shorter (2.00 Å), with an NH orientation pointing much more directly to the carbonyl oxygen. The spectroscopic result is a triad of NH stretch fundamentals composed of two higher-frequency, nearly degenerate fundamentals due to the C7 H-bonds and a single C14 NH stretch shifted down in frequency by an additional 50 cm^{-1}; the predicted pattern matches observation, although the calculated shifts are systematically too small.

The highly folded structures of these C7/C7/C14 cycles, with their γ-peptide reverse turns, bear some resemblance to the amide-stacked structure that was observed in Ac-γ^2-hPhe-NHMe. In fact, close inspection of the triamide cycles in Figure 6 reveals that the two terminal amide groups are both in an antiparallel orientation with respect to the interior amide group, much as they would be in amide stacking. However, in forming a C14 H-bond with one another, the two terminal amides are prevented from engaging in full antiparallel amide stacking with the central amide by each other's presence. Instead, they participate in two C7 H-bonds with the central amide group, held in positions that are likely still stabilized to some degree by amide stacking.

Table 3 compares the dihedral angles of the γ-peptide backbones of the two assigned C7/C7/C14 structures with those of the stacked conformer of Ac-γ^2-hPhe-NHMe. The (θ, ζ) dihedral angles for the interior → C-terminal reverse turn of Ac-γ^2-hAla-γ^2-hPhe-NHMe (C) and the N-term → interior turn of Ac-γ^2-hPhe-γ^2-hAla-NHMe are similar to those present in the amide-stacked conformation, but the H-bonds hinder full collapse into the antiparallel arrangement, leading to differences of about 45−55° in ϕ as it opens up to form the C14 H-bond.

It is interesting to note that the calculated dihedral angles present in the C7/C7/C14 structures are not among those reported for the repeating units of the γ-peptide hexamers of Baldauf et al.[21] The fact that structures such as this were not characterized in the previous computational study argues for the importance of experimental studies capable of uncovering and characterizing unanticipated structures. Furthermore, new structural motifs such as the C7/C7/C14 cycle and amide-stacking can serve as testing grounds for those developing new density functionals[44,45,55] or molecular mechanics force fields,[68−71] where multiple intramolecular interactions (electrostatics, dispersion, charge transfer, Pauli repulsion) must be accurately computed.

To drive this point home, Figure 8 compares the experimental RIDIR spectrum of the C7/C7/C14 structures of Ac-γ^2-hPhe-γ^2-hAla-NHMe and Ac-γ^2-hAla-γ^2-hPhe-NHMe with the results of harmonic frequency calculations and IR intensities from B3LYP/6-31+G(d), M05-2X/6-311++G(d,p), M06-2X/6-311++G(d,p), and ωB97x-D/6-311++G(d,p) calculations. Scale factors (included in the figure caption) are chosen so as to bring the free amide NH stretch present in C9/C9 or C9/C14 structures into agreement with experiment. The B3LYP calculations represent a standard level of theory often used with success in cases where electrostatic interactions (e.g., H-bonding) dominate.[27−29,72−74] However, the B3LYP calculations fail to even qualitatively capture the positions or intensity patterns present in the C7/C7/C14 cycles, with its complex balance of electrostatic and dispersive interactions. The dispersion-corrected M05-2X,[50−52] M06-2X, and ωB97x-D[55] functionals perform markedly better, with the latter level of theory showing the closest correspondence with experiment, both in frequency and in intensity pattern. Nevertheless, no level of theory captures the full range of intramolecular interactions, leading to calculated frequencies too high by ∼25−50 cm^{-1}. These changes in vibrational frequency reflect differences in the optimized structures at the three levels of theory, as summarized in Table 4. Note that the M05-2X, M06-2X, and ωB97x-D calculations predict much smaller NH···O H-bond distances than those of B3LYP, and drop the energy of the C7/C7/C14 structure to within a couple of kJ/mol of the global minimum C9/C9 sequential double ring (Table 2). This implies an important role for dispersive interactions in stabilizing the C7/C7/C14 H-bonded cycle, and highlights these conformers as especially good targets for those developing state-of-the-art theoretical methods aimed at improving dispersion corrections.

3. Amide Tristacks. Once the similar dihedral angles between the C7/C7/C14 cycle and amide stacked structures are recognized, it is natural to speculate on the possibility of forming a "tri-stacked" structure in which the second reverse turn brings the final amide group on the other side of the interior amide, where

Table 4. Energies Relative to the C9/C9(a) Global Minimum and Hydrogen Bond Distances Calculated by the Four Different Density Functionals Employed in This Paper for the C7/C7/C14(g-) Structures of Ac-γ^2-hPhe-γ^2-hAla-NHMe and Ac-γ^2-hAla-γ^2-hPhe-NHMe

level of theory	relative energy (kJ/mol)	C7 $r_{(H\cdots O)}$[a]	C7 $r_{(H\cdots O)}$[b]	C14 $r_{(H\cdots O)}$
		Ac-γ^2-hPhe-γ^2-hAla-NHMe (C) C7/C7/C14(g-)		
B3LYP/6-31+G(d)	14.06	2.329	2.198	2.173
M05-2X/6-311++G(d,p)	2.91	2.166	2.166	2.057
M06-2X/6-311++G(d,p)	2.63	2.161	2.178	2.023
ωB97X-D/6-311++G(d,p)	1.49	2.158	2.136	2.008
		Ac-γ^2-hAla-γ^2-hPhe-NHMe (C) C7/C7/C14(g-)		
B3LYP/6-31+G(d)	12.07	2.209	2.450	2.058
M05-2X/6-311++G(d,p)	0.90	2.152	2.232	2.027
M06-2X/6-311++G(d,p)	0.01	2.147	2.209	2.020
ωB97X-D/6-311++G(d,p)	0.32	2.123	2.259	1.993

[a] Values for the C7 composed of the amide amide H-bond enclosed by the interior C═O and N-terminal NH group. [b] Values for the C7 composed of the amide amide H-bond enclosed by the C-terminal C═O and interior NH group.

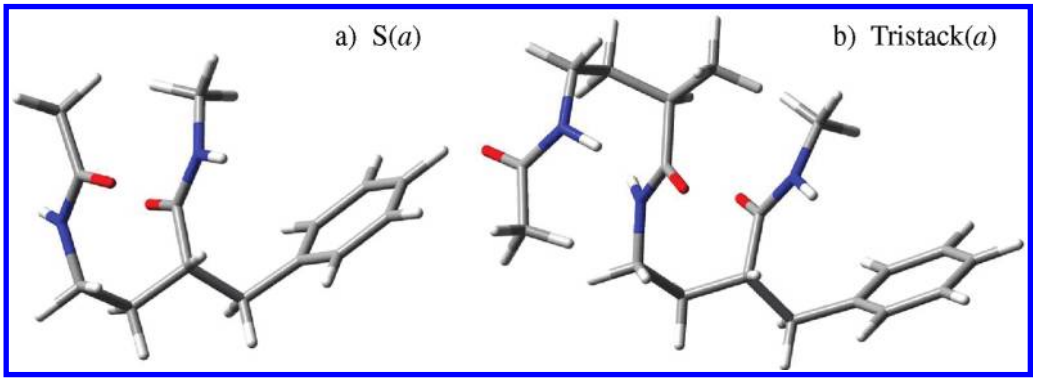

Figure 9. (a) Ac-γ^2-hPhe-NHMe amide stacked structure S(a). (b) Ac-γ^2-hAla-γ^2-hPhe-NHMe amide tristacked structure S′/S(a), which is not observed experimentally. See text for further discussion.

the N-terminal and C-terminal amide groups approach the interior amide group from opposite sides. We have searched for and located two tristacked structures of Ac-γ^2-hAla-γ^2-hPhe-NHMe (both with the phenyl ring in the anti position) with relative energies of 23.2 and 27.9 kJ/mol above the C9/C9(a) global minimum, significantly greater than the 1.42 kJ/mol difference between S(a) and C9(g−) in Ac-γ^2-hPhe-NHMe. Figure 9 presents a side-on view of the lowest-energy tristacked structure of Ac-γ^2-hAla-γ^2-hPhe-NHMe (Figure 9b) predicted by theory, comparing it with the amide-stacked Ac-γ^2-hPhe-NHMe structure S(a) (Figure 9a).

The dihedral angles present in these two tristacked structures (labeled S′/S and S/S) are included in Table 3. Note first the close similarity in dihedral angles between C7/C7/C14 and S′/S, with the change in sign between the first set of C7 and S′ dihedrals reflecting the opposite direction of the turn in forming the cycle relative to the tristack.

Second, whereas the two sets of dihedrals in the two layers of stacking are the same in S/S(a), in S′/S(a) they are not. These dihedral angles differ by whether the γ^3 carbon forms a boat or chair conformation with the NH/C═O groups closest to it, much as in the different C7 rings of the C7/C7/C14 cycle. We label the tristack structure containing these two stacking types as S′/S(a) tristack in acknowledgment of that fact. It is worth noting that an S′(a) stack can be formed in Ac-γ^2-hPhe-NHMe (Table 3), but it is less stable than S(a) by 16.7 kJ/mol due to an unfavorable interaction of the C-terminal amide C═O group with the aromatic ring. When the phenyl ring is removed, S and S′ stacks differ by 6.3 kJ/mol, with S lower than S′.

The other triamide stack is an S/S(a) structure, which is destabilized by ∼5 kJ/mol relative to S′/S(a) by an unfavorable steric interaction of the alanine side chain in the γ^2-position with the C-terminal amide group, which disrupts stacking. Removing this steric interaction by moving the position of methyl substitution to the γ^3 or γ^4 carbon or by changing the chirality of the γ^2 carbon may prove a worthwhile design strategy for stabilizing high-order stacked structures in future work.

B. FMO/PIEDA Analysis. In our previous studies of Ac-γ^2-hPhe-NHMe,[19] quantitative predictions for the various contributions to the intramolecular interactions present in the H-bonded and amide stacked structures were obtained by employing the systematic fragmentation/effective fragmentation potential method (SFM/EFP).

Fragment molecular orbital (FMO) with pair interaction energy decomposition analysis (PIEDA)[37] is a method that provides an alternative scheme to SFM/EFP for cutting a large molecule into fragments and then breaking the total energy into nonbonded and through-bond contributions. Figure 10 compares SFM/EFP and FMO-PIEDA noncovalent interactions in the diamide Ac-γ^2-hPhe-NHMe. The total noncovalent energies

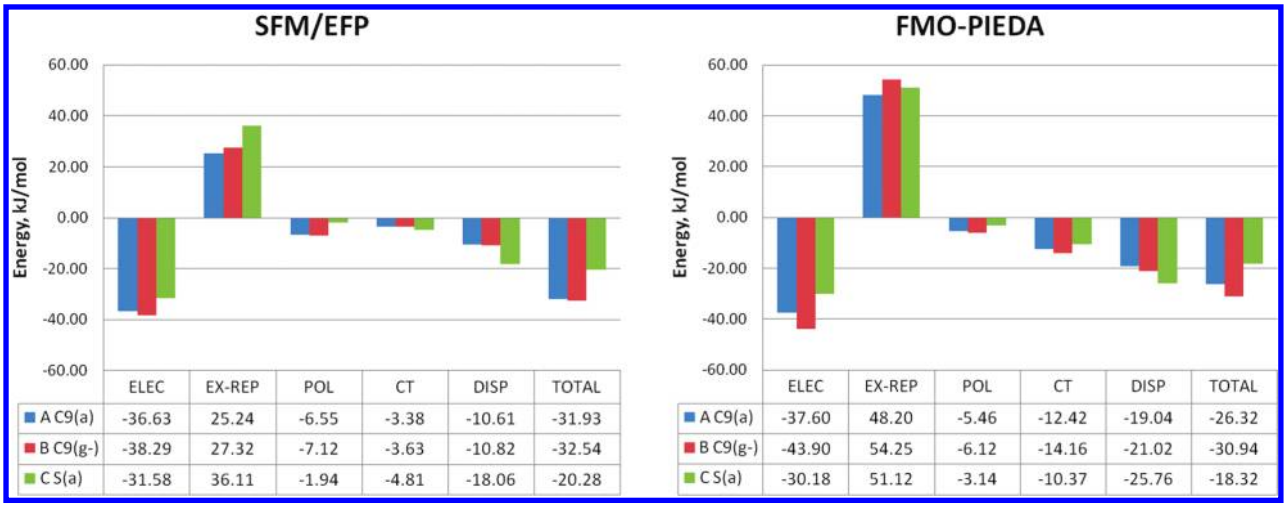

Figure 10. Comparison of SFM/EFP and FMO-PIEDA noncovalent energies for Ac-γ^2-hPhe-NHMe. All energies in kJ/mol.

Table 5. Nonbonded Interactions (kJ/mol) in Ac-γ^2-hPhe-γ^2-hAla-NHMe and Ac-γ^2-hAla-γ^2-hPhe-NHMe Triamides by FMO-PIEDA

	Ac-γ^2-hPhe-γ^2-hAla-NHMe				Ac-γ^2-hAla-γ^2-hPhe-NHMe			
	A	B	C	D	A	B	C	D[c]
nonbonded contributions	C9/C9(a)	C9/C9(g-)	C7/C7/C14(g-)	C9/C9(g+)	C9/C9(a)	C9/C9(a)	C7/C7/C14(g-)	S(a)
electrostatics	−86.6	−91.4	−95.5	−86.5	−90.4	−65.1	−103.0	56.8
exchange repulsion	111.9	116.4	114.9	102.6	114.9	92.9	128.4	99.7
elec + ex-rep	25.2	24.9	19.5	16.0	24.5	27.8	25.4	43.0
charge transfer	−30.8	−31.9	−36.0	−34.5	−32.2	−25.4	−40.4	21.6
polarization	−12.9	−13.4	−15.5	−11.4	−13.2	−9.5	−16.3	−6.5
dispersion	−39.0	−40.1	−46.9	−46.4	−39.6	−39.9	−54.6	−49.5
total nonbonded energy	−57.4	−60.4	−78.8	−76.3	−60.5	−47.0	−85.8	−34.6
relative nonbonded energy	28.4	25.4	7.0	9.5	25.4	38.9	0.0	51.2
total relative energy[a]	6.5	8.0	10.1	13.9	3.5	14.4	0.0	26.6
relative through-bond energy[b]	−21.9	17.4	3.1	4.4	−21.8	−24.5	0.0	−24.6

[a] MP2/6-31G* relative electronic energies (without ZPE correction) at the ωB97X-D/6-311++G(d,p) optimized geometries. [b] Difference between total relative and relative nonbonded energies ascribable to through bond contributions to the relative stabilities. [c] Not observed experimentally.

in both methods are split into electrostatic, exchange−repulsion, polarization, charge transfer, and dispersion terms. Although the absolute values of the energy terms are somewhat different in the two schemes, mainly due to differences in the way in which the diamide was cut into noncovalent fragments (see Computational Methods for details), general trends are preserved. In particular, both SFM/EFP and FMO-PIEDA predict that the stacked conformer C S(a) has weaker electrostatic and stronger dispersion interactions, and smaller total noncovalent energy than A and B conformers with C9 H-bonded cycles. Weaker noncovalent interactions in the stacked conformer are partly compensated by a decreased through-bond strain, as discussed in the previous study.[19]

Table 5 summarizes the nonbonded contributions to the assigned conformer structures of Ac-γ^2-hPhe-γ^2-hAla-NHMe and Ac-γ^2-hAla-γ^2-hPhe-NHMe triamides, calculated with FMO-PIEDA. The triamides are represented by three unconnected fragments each containing an amide group. The fragmentation for Ac-γ^2-hPhe-γ^2-hAla-NHMe and Ac-γ^2-hAla-γ^2-hPhe-NHMe is shown in the Supporting Information. Decomposition of the total noncovalent interactions into pairwise components is shown in Figure 11. It is worth noting that a part of the polarization energy and mixed polarization-dispersion term cannot be decomposed into pairwise interactions. These destabilizing many-body contributions are not shown in Figure 11 but are included into the total polarization and dispersion energies in Table 5. For comparison, energy decompositions of the three conformers of Ac-γ^2-hPhe-NHMe diamide are also shown.

Three structures with C9/C9 double rings, Ac-γ^2-hPhe-γ^2-hAla-NHMe (A, B) and Ac-γ^2-hAla-γ^2-hPhe-NHMe (A), have very similar patterns of nonbonded interactions. The distinguishing characteristic of these conformers is the presence of two strong H-bonds, each of which is dominated by the electrostatic term. Exchange−repulsion energy cancels the electrostatics, but a sum of dispersion, charge transfer, and polarization make these structures bound by ∼57−60 kJ/mol, about twice as big as the total noncovalent interactions in H-bonded dipeptides. A small additional stabilizing contribution in these structures (8−12 kJ/mol) originates from the interaction of a pair of fragments (fragments 1 and 3, see Figure 11) that are not involved in H-bonding with each other.

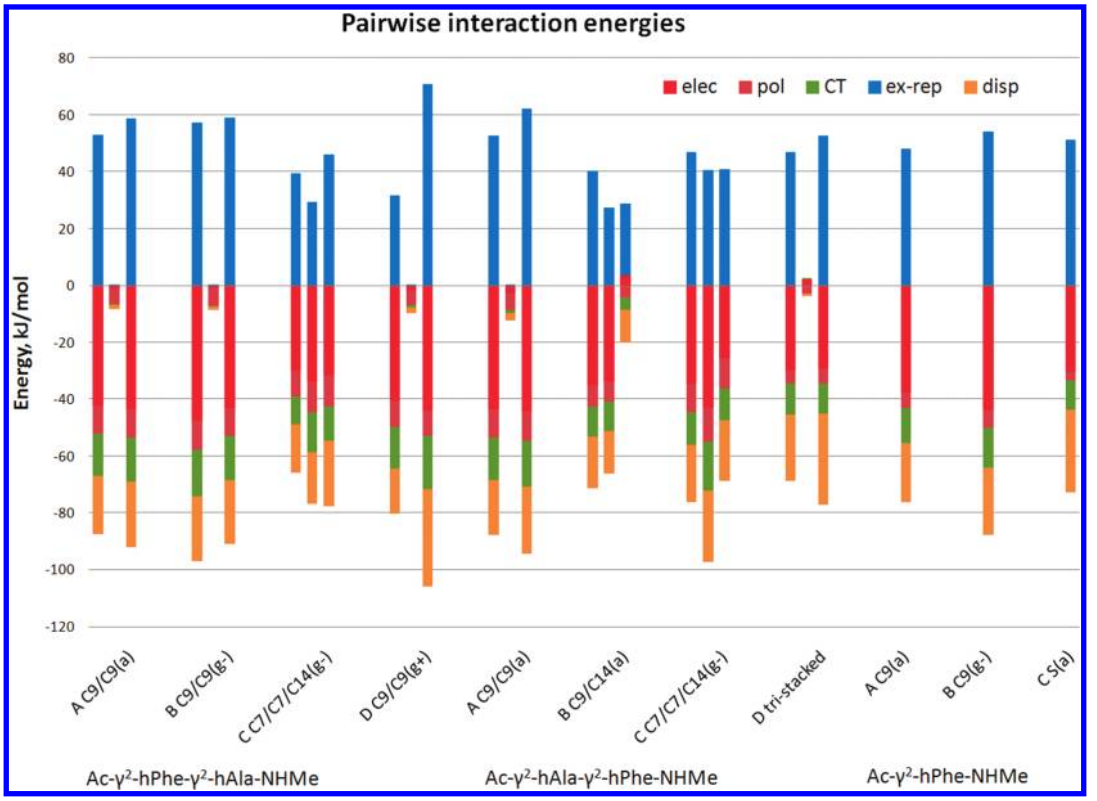

Figure 11. Pairwise noncovalent energies by FMO-PIEDA for Ac-γ^2-hPhe-γ^2-hAla-NHMe, Ac-γ^2-hAla-γ^2-hPhe-NHMe, and Ac-γ^2-hPhe-NHMe conformers. For triamide conformers, interactions between fragments 1−2, 1−3, and 2−3 (from left to right) are shown.

The Ac-γ^2-hPhe-γ^2-hAla-NHMe (D) conformer also possesses two C9/C9 H-bonds but is additionally stabilized by dispersive interactions of the phenyl ring with the amide chain (Figure 5b). As a result, the total noncovalent energy in Ac-γ^2-hPhe-γ^2-hAla-NHMe(D) is ∼12 kJ/mol more attractive than that in the other C9/C9 conformers.

In agreement with spectroscopic observations, the bifurcated structure Ac-γ^2-hAla-γ^2-hPhe-NHMe (B) with C9/C14 H-bonding pattern has two weak H-bonds. However, smaller electrostatic attraction in these longer H-bonds (Table 5 and Figure 11) is compensated by smaller exchange−repulsion. Nevertheless, the longer H-bonds result in smaller charge transfer and polarization components, leading to an overall weaker noncovalent interaction in the C9/C14 conformer. Equally important, as is revealed in Figure 11, this structure exhibits an anticooperative destabilizing interaction between the two donor fragments involved in the bifurcated H-bonds (fragments 2 and 3).

The C7/C7/C14 structures Ac-γ^2-hPhe-γ^2-hAla-NHMe (C) and Ac-γ^2-hAla-γ^2-hPhe-NHMe (C) contain three amide−amide H-bonds. This leads to attractive nonbonded interactions among all three fragments, as is obvious from the stick diagrams in Figure 11. These more distorted H-bonds are slightly weaker than the H-bonds in the C9 cycles, but the presence of three of them leads to stronger total noncovalent interactions than in the C9/C9 double-ring structures. In fact, this trend holds for each of the components of the total nonbonded energy individually. As a result of this cooperative behavior, the C7/C7/C14 conformers have the lowest noncovalent energies of any of the observed conformers (−85.8 and −78.8 kJ/mol, respectively).

It is worth considering the S′/S(a) tristacked structure found by the calculations, to understand why it is higher in energy and not observed experimentally. Comparison of the contributions to the nonbonded interactions in the tristacked conformer with the amide-stacked structure in Ac-γ^2-hPhe-NHMe shows that each of the two stacking interactions (1−2 and 2−3) in Ac-γ^2-hAla-γ^2-hPhe-NHMe is nearly identical in energy composition to the single stack S(a) in Ac-γ^2-hPhe-NHMe (Figure 11). As shown in Table 5, compared to the case of conformers with H-bonds, dispersion forces make up a larger percentage of the noncovalent interactions in the tristacked conformer, whereas electrostatics, polarization, and charge transfer are significantly weaker. This is in agreement with the character of the noncovalent interactions observed in the stacked diamide (Figure 10).

However, the total noncovalent energy in the stacked triamide (−34.6 kJ/mol) is much less attractive than that in most of the H-bonded conformers (−47.0 to −85.8 kJ/mol). This is because the tristacked structure lacks any cooperative effects; i.e., the total noncovalent energy is just a sum of energies of two pairs of stacked dimers, with the interaction between fragments 1 and 3 near zero. The C9/C9 sequential double rings also are primarily stabilized by nearest-neighbor interactions (1−2 and 2−3); however, the 1−3 interactions are additionally stabilizing by ∼8−12 kJ/mol. Thus, in contrast to the diamide, cooperativity starts to play an important role in stabilization of the triamides and may increase still further in importance in larger γ-peptides.

The above analysis provides a qualitative picture of nonbonded interactions in the γ-triamides. However, structures with favorable nonbonded interactions may experience increased through-bond strain and as a result be higher in energy than the less-strained structures. To estimate the through-bond strain, the total relative energies of the conformers was compared with their nonbonded energies. The obtained energy difference

provides a measure of the relative through-bond strain of the conformers. For consistency with FMO results (obtained at the MP2/6-31G* level of theory), the MP2/6-31G* level of theory was used in calculating the total energies as well. As mentioned previously, the differences between MP2/6-31G* and ωB97X-D/6-311++G(d,p) relative electronic energies do not exceed 3.2 kJ/mol.

As shown in Table 5, the C7/C7/C14 structures are destabilized by a through-bond strain with respect to the C9/C9 double-ring structures. This is understandable because a formation of C7 rings necessarily results in a more strained backbone. Among C9/C9 structures, Ac-γ^2-hPhe-γ^2-hAla-NHMe (D) has the highest strain energy that counteracts its favorable dispersive interactions. The C9/14 bifurcated conformer and the tristacked conformer have similarly low through-bond energies. However, compared to the two lowest C9/C9 structures, Ac-γ^2-hPhe-γ^2-hAla-NHMe (A,B), the tristacked structure has no additional through-bond stabilization, unlike the diamide, where there was a significant lowering of the steric strain in the amide stacked versus C9 structures.

C. Natural Bond Orbital (NBO) Analysis. Raines and co-workers[38,39] have recently proposed a potentially important role for stabilizing n → π* interactions between amide groups in polypeptides and proteins, using natural bond orbital (NBO) analysis.[66,75] In that work, the focus was on interactions between two C═O groups, in which a nonbonded oxygen lone pair of one C═O donates to the π* orbital on an adjacent C═O group. It is worth briefly considering amide stacking in terms of an NBO analysis to compare with this work. In contrast to the FMO-PIEDA calculations just considered in section IV.B, the NBO analysis focuses attention on charge transfer contributions arising from orbital overlap between interacting amide groups.

An NBO analysis was carried out on the optimized structures of Ac-γ^2-hPhe-NHMe, Ac-γ^2-hPhe-γ^2-hAla-NHMe, and Ac-γ^2-hAla-γ^2-hPhe-NHMe at the ωB97X-D/6-311++G(d,p) level of theory. Here we focus attention on the amide-stacked structures and the C7/C7/C14 cycles, where a close approach of amide groups at oblique angles gives rise to n → π* interactions between them. However, unlike the C═O···C═O interactions noted by Raines et al.,[38,39] the n → π* interactions between stacked amide group in our molecules occur between the amide nitrogen lone pair of one amide and the π* orbital on the C═O group of the other (Supporting Information). The amide-stacked structure of Ac-γ^2-hPhe-NHMe contains two such n → π* interactions. To assess the strength of these interactions, we use the second-order perturbation energy ($E_{(2)}$) calculated for the interaction between each nitrogen lone pair and the corresponding antibonding (BD*(2)) orbital of a C═O group.

In Ac-γ^2-hPhe-NHMe, the strength of the amide-stacked n → π* interactions are 5.89 and 2.97 kJ/mol. The stronger interaction takes place between N-terminal nitrogen and the C-terminal C═O group, which is calculated to be closer in proximity (2.93 Å) than in the other N···C═O pair (3.12 Å). Both the distances and interaction energies are in ranges similar to those found for the C═O···C═O interactions by Raines and co-workers.[38,39]

In the C7/C7/C14 structures of Ac-γ^2-hPhe-γ^2-hAla-NHMe and Ac-γ^2-hAla-γ^2-hPhe-NHMe, we noted previously that adjacent amide groups are in a "frustrated" amide stacking configuration, in which both terminal amide groups fold back toward an amide stacking configuration but are kept from doing so by formation of a C14 H-bond between them. Despite this, the distances between the interior nitrogen atom and the C-terminal C═O group of Ac-γ^2-hPhe-γ^2-hAla-NHMe and Ac-γ^2-hAla-γ^2-hPhe-NHMe are 2.93 and 3.01 Å, respectively. On the basis of these distances, and with extrapolation from results mentioned in the preceding paragraph, one may anticipate interaction energies in these cases of ∼6 kJ/mol. However, the energies found here are about half that size (3.0 and 3.8 kJ/mol). These lower-than-expected energies are hypothesized to be a consequence of the amide group participating in both amide-stacking and C7 H-bonding, and therefore not in an optimal geometry for the n → π* interaction.

Thus, from the vantage point of NBO analysis, amide stacking interactions involve a distinctive type of n → π* interaction between the C═O and NH groups facilitated by the close approach of the two amide groups in an antiparallel stacked arrangement. It would be interesting to see the extent to which this interaction might be present in naturally occurring proteins or other types of synthetic foldamers.

V. CONCLUSIONS

The conformational preferences present in the γ-peptide triamides studied here may be seen as natural extensions of those found in α-, β-, and α/β-peptide analogs. In each case, the conformations observed can be categorized broadly in terms of three structural types: sequential double H-bonded rings, bifurcated double H-bonded rings, and single H-bonded rings. In the α-peptides Ac-Phe-Ala-NH_2 and Ac-Ala-Phe-NH_2, studied in detail by Mons and co-workers,[34,72,76] conformer population was distributed over C5/C7 bifurcated double ring, C7/C7 sequential double ring, and C10 single ring H-bonded families. In the β^3-peptides Ac-β^3-hPhe-β^3-hAla-NHMe and Ac-β^3-hAla-β^3-hPhe-NHMe, studied by our group,[27,28] C6/C6 and C8/C8 sequential double rings and C10 single rings were observed. In the heterogeneous α/β-peptide foldamers Ac-Phe-β^3-hAla-NHMe and Ac-β^3-hAla-Phe-NHMe sequential double rings (C8/C7 or C6/C5), single rings (C11), and bifurcated double rings (C5/C8) were observed.[29,30]

In the γ^2-peptides that are the subject of the present work, C9/C9 sequential double rings and C9/C14 bifurcated double rings were both observed. The C9/C9 sequential rings dominated the conformer population, pairing together two strong H-bonds between adjacent amide groups. The C9/C14 bifurcated double ring structure is in many ways a modified single-ring C14 structure in which the large single ring is further stabilized by formation of a second H-bond from the interior amide group with the N-terminal C═O group, made possible by the flexibility of the γ-peptide backbone.

Despite similarities to their smaller α-, β-, and α/β-peptide analogs, the γ-peptides have shown themselves to be capable of new structural possibilities enabled by the larger separation and increased flexibility of the three-carbon connector between amide groups. In fact, a primary motivation for the present study was to determine whether the new structural motif of amide stacking[19] uncovered in the diamide Ac-γ^2-hPhe-NHMe would show itself in some way in the conformational preferences of the triamide γ-peptides. Although no tristacked structure was observed experimentally, the C7/C7/C14 H-bonded cycle makes use of the γ-peptide backbone structure to collapse in on itself in forming a H-bonded cycle involving all three amide groups, the first of its kind in natural peptides or synthetic foldamers. The comparison of the experimental results with theory has provided a basis for the conformational preferences and also uncovered deficiencies in the ability even of dispersion-corrected functionals

to fully account for the delicate balance of intramolecular interactions present in these cycles.

Theoretical developments such as SFM/EFP,[33,64,65] FMO-PIEDA,[58] NBO,[66] and AIMS[77,78] analysis all purport to capture key intramolecular interactions at play in molecules such as this. Single-conformation studies such as those presented here provide a rich and incisive testing ground for these theories and others. Here we have taken a first step in this direction in carrying out FMO-PIEDA and NBO calculations, which provide complementary views.

Given the structural surprises found in the γ-peptides studied to date (amide stacking and triamide H-bonded cycle), it seems important to follow this structural development to larger γ-peptide foldamers. Studying larger oligomers as neutral species will require laser desorption to bring these molecules into the gas phase. The possibility of studying even larger foldamers as ions, using the techniques pioneered by Rizzo and co-workers,[79] is another avenue worth pursuing vigorously.

■ ASSOCIATED CONTENT

Supporting Information. Table S1−S3: Comparison of relative energies of conformers and NH stretch frequencies for various dispersion-corrected functionals. Figures S1−S7: Comparison of experimental RIDIR spectra with the predictions of calculations at these levels of theory. Figure S8: Depiction of the low-frequency vibrational mode of C9/C9(a) that dominates the spectrum. Figure S9: Visualization of the fragmentation used in FMO-PIEDA for calculating nonbonded interactions. Figure S10: Orbitals calculated to interact via natural bond orbital analysis in the amide stacked conformer of Ac-γ^2-hPhe-NHMe. Tables S4 and S5: Cartesian coordinates. This information is available free of charge via the Internet at http://pubs.acs.org.

■ AUTHOR INFORMATION

Present Addresses

[‡]SCHOTT North America, Inc. 400 York Ave., Duryea, PA 18642, U.S.A.

[§]Ruhr University Bochum, Department of Physical Chemistry 2, D-44780 Bochum, Germany.

[∥]The Dow Chemical Company, Formulation Science, 1712 Bldg./23-1, Midland, MI 48667, U.S.A.

■ ACKNOWLEDGMENT

W.H.J., E.G.B., C.W.M., J.C.D., and T.S.Z. acknowledge support for this research from the National Science Foundation (NSF-CHE0909619). C.W.M. also thanks the "Deutsche Akademie der Naturforscher Leopoldina" for a postdoctoral scholarship (grant number BMBF-LPD 9901/8-159 of the "Bundesministerium für Bildung und Forschung"). S.H.G. and L.G. were supported by NSF grant CHE-0848847. D.K. and L.V.S. acknowledge support from NSF grant CHE-CAREER-0955419.

■ REFERENCES

(1) Gellman, S. H. *Acc. Chem. Res.* **1998**, *31*, 173.
(2) Cheng, R. P.; Gellman, S. H.; DeGrado, W. F. *Chem. Rev.* **2001**, *101*, 3219.
(3) Seebach, D.; Gardiner, J. *Acc. Chem. Res.* **2008**, *41*, 1366.
(4) Horne, W. S.; Gellman, S. H. *Acc. Chem. Res.* **2008**, *41*, 1399.
(5) Guo, L.; Chi, Y. G.; Almeida, A. M.; Guzei, I. A.; Parker, B. K.; Gellman, S. H. *J. Am. Chem. Soc.* **2009**, *131*, 16018.
(6) Chi, Y.; Guo, L.; Kopf, N. A.; Gellman, S. H. *J. Am. Chem. Soc.* **2008**, *130*, 5608.
(7) Garcia-Garcia, P.; Ladepeche, A.; Halder, R.; List, B. *Angew. Chem., Int. Ed.* **2008**, *47*, 4719.
(8) Hayashi, Y.; Itoh, T.; Ohkubo, M.; Ishikawa, H. *Angew. Chem., Int. Ed.* **2008**, *47*, 4722.
(9) Nodes, W. J.; Nutt, D. R.; Chippindale, A. M.; Cobb, A. J. A. *J. Am. Chem. Soc.* **2009**, *131*, 16016.
(10) Wiesner, M.; Revell, J. D.; Tonazzi, S.; Wennemers, H. *J. Am. Chem. Soc.* **2008**, *130*, 5610.
(11) Guo, L.; Almeida, A. M.; Zhang, W.; Reidenbach, A. G.; Choi, S. H.; Guzei, I. A.; Gellman, S. H. *J. Am. Chem. Soc.* **2010**, *132*, 7868.
(12) Hanessian, S.; Luo, X. H.; Schaum, R.; Michnick, S. *J. Am. Chem. Soc.* **1998**, *120*, 8569.
(13) Hintermann, T.; Gademann, K.; Jaun, B.; Seebach, D. *Helv. Chim. Acta* **1998**, *81*, 983.
(14) Seebach, D.; Beck, A. K.; Bierbaum, D. J. *Chem. Biodivers.* **2004**, *1*, 1111.
(15) Seebach, D.; Brenner, M.; Rueping, M.; Jaun, B. *Chem.—Eur. J.* **2002**, *8*, 573.
(16) Seebach, D.; Brenner, M.; Rueping, M.; Schweizer, B.; Jaun, B. *Chem. Commun.* **2001**, *2*, 207.
(17) Seebach, D.; Hook, D. F.; Glattli, A. *Biopolymers* **2006**, *84*, 23.
(18) Vasudev, P. G.; Chatterjee, S.; Ananda, K.; Shamala, N.; Balaram, P. *Angew. Chem., Int. Ed.* **2008**, *47*, 6430.
(19) James, W. H., III; Müller, C. W.; Buchanan, E. G.; Nix, M. G. D.; Guo, L.; Roskop, L.; Gordon, M. S.; Slipchenko, L. V.; Gellman, S. H.; Zwier, T. S. *J. Am. Chem. Soc.* **2009**, *131*, 14243.
(20) Araghi, R. R.; Jackel, C.; Colfen, H.; Salwiczek, M.; Volkel, A.; Wagner, S. C.; Wieczorek, S.; Baldauf, C.; Koksch, B. *Chembiochem* **2010**, *11*, 335.
(21) Baldauf, C.; Gunther, R.; Hofmann, H. J. *Helv. Chim. Acta* **2003**, *86*, 2573.
(22) Baldauf, C.; Gunther, R.; Hofmann, H. J. *Angew. Chem., Int. Ed.* **2004**, *43*, 1594.
(23) Baldauf, C.; Gunther, R.; Hofmann, H. J. *Biopolymers* **2005**, *80*, 675.
(24) Baldauf, C.; Gunther, R.; Hofmann, H. J. *J. Org. Chem.* **2006**, *71*, 1200.
(25) Koksch, B.; Araghi, R. R.; Baldauf, C.; Pisabarro, M. T. *Amino Acids* **2009**, *37*, 42.
(26) Rezaei, A. R.; Baldauf, C.; Koksch, B. *J. Pept. Sci.* **2008**, *14*, 175.
(27) Baquero, E. E.; James, W. H.; Choi, S. H.; Gellman, S. H.; Zwier, T. S. *J. Am. Chem. Soc.* **2008**, *130*, 4784.
(28) Baquero, E. E.; James, W. H.; Choi, S. H.; Gellman, S. H.; Zwier, T. S. *J. Am. Chem. Soc.* **2008**, *130*, 4795.
(29) James, W. H., III; Baquero, E. E.; Choi, S. H.; Gellman, S. H.; Zwier, T. S. *J. Phys. Chem. A* **2010**, *114*, 1581.
(30) James, W. H., III; Baquero, E. E.; Shubert, V. A.; Choi, S. H.; Gellman, S. H.; Zwier, T. S. *J. Am. Chem. Soc.* **2009**, *131*, 6574.
(31) Nelson, R.; Sawaya, M. R.; Balbirnie, M.; Madsen, A. O.; Riekel, C.; Grothe, R.; Eisenberg, D. *Nature* **2005**, *435*, 773.
(32) Buchanan, E. G.; James, W. H.; Gutberlet, A.; Dean, J. C.; Guo, L.; Gellman, S. H.; Zwier, T. S. *Faraday Discuss.* **2011**, DOI: 10.1039/C1FD00001B.
(33) Gordon, M. S.; Mullin, J. M.; Pruitt, S. R.; Roskop, L. B.; Slipchenko, L. V.; Boatz, J. A. *J. Phys. Chem. B* **2009**, *113*, 9646.
(34) Mons, M.; Piuzzi, F.; Dimicoli, I. *Actual. Chim.* **2007**, 19.
(35) Fricke, H.; Funk, A.; Schrader, T.; Gerhards, M. *J. Am. Chem. Soc.* **2008**, *130*, 4692.
(36) Fricke, H.; Gerlach, A.; Unterberg, C.; Rzepecki, P.; Schrader, T.; Gerhards, M. *Phys. Chem. Chem. Phys.* **2004**, *6*, 4636.
(37) Fedorov, D. G.; Kitaura, K. *J. Comput. Chem.* **2007**, *28*, 222.
(38) Bartlett, G. J.; Choudhary, A.; Raines, R. T.; Woolfson, D. N. *Nat. Chem. Biol.* **2010**, *6*, 615.

(39) Jakobsche, C. E.; Choudhary, A.; Miller, S. J.; Raines, R. T. *J. Am. Chem. Soc.* **2010**, *132*, 6651.
(40) Zwier, T. S. *J. Phys. Chem. A* **2006**, *110*, 4133.
(41) Page, R. H.; Shen, Y. R.; Lee, Y. T. *J. Chem. Phys.* **1988**, *88*, 5362.
(42) Zwier, T. S. *Annu. Rev. Phys. Chem.* **1996**, *47*, 205.
(43) Zwier, T. S. *J. Phys. Chem. A* **2001**, *105*, 8827.
(44) Weiner, P. K.; Kollman, P. A. *J. Comput. Chem.* **1981**, *2*, 287.
(45) Halgren, T. A. *J. Comput. Chem.* **1996**, *17*, 490.
(46) Mohamadi, F.; Richards, N. G. J.; Guida, W. C.; Liskamp, R.; Lipton, M.; Caufield, C.; Chang, G.; Hendrickson, T.; Still, W. C. *J. Comput. Chem.* **1990**, *11*, 440.
(47) Becke, A. D. *J. Chem. Phys.* **1993**, *98*, 5648.
(48) Lee, C. T.; Yang, W. T.; Parr, R. G. *Phys. Rev. B* **1988**, *37*, 785.
(49) Frisch, M. J.; Trucks, G. W.; Schlegel, H. B.; Scuseria, G. E.; Robb, M. A.; Cheeseman, J. R.; Scalmani, G.; Barone, V.; Mennucci, B.; Petersson, G. A.; Nakatsuji, H.; Caricato, M.; Li, X.; Hratchian, H. P.; Izmaylov, A. F.; Bloino, J.; Zheng, G.; Sonnenberg, J. L.; Hada, M.; Ehara, M.; Toyota, K.; Fukuda, R.; Hasegawa, J.; Ishida, M.; Nakajima, T.; Honda, Y.; Kitao, O.; Nakai, H.; Vreven, T.; Montgomery, J. A., Jr.; Peralta, J. E.; Ogliaro, F.; Bearpark, M.; Heyd, J. J.; Brothers, E.; Kudin, K. N.; Staroverov, V. N.; Kobayashi, R.; Normand, J.; Raghavachari, K.; Rendell, A.; Burant, J. C.; Iyengar, S. S.; Tomasi, J.; Cossi, M.; Rega, N.; Millam, N. J.; Klene, M.; Knox, J. E.; Cross, J. B.; Bakken, V.; Adamo, C.; Jaramillo, J.; Gomperts, R.; Stratmann, R. E.; Yazyev, O.; Austin, A. J.; Cammi, R.; Pomelli, C.; Ochterski, J. W.; Martin, R. L.; Morokuma, K.; Zakrzewski, V. G.; Voth, G. A.; Salvador, P.; Dannenberg, J. J.; Dapprich, S.; Daniels, A. D.; Farkas, Ö.; Foresman, J. B.; Ortiz, J. V.; Cioslowski, J.; Fox, D. J. *Gaussian 09*; Gaussian, Inc.: Wallingford, CT, 2009.
(50) Zhao, Y.; Truhlar, D. G. *J. Chem. Theory Comput.* **2006**, *2*, 1009.
(51) Zhao, Y.; Truhlar, D. G. *J. Chem. Theory Comput.* **2007**, *3*, 289.
(52) Zhao, Y.; Truhlar, D. G. *Acc. Chem. Res.* **2008**, *41*, 157.
(53) Zhao, Y.; Truhlar, D. G. *Theor. Chem. Acc.* **2008**, *120*, 215.
(54) Zhao, Y.; Truhlar, D. G. *J. Chem. Theory Comput.* **2008**, *4*, 1849.
(55) Chai, J. D.; Head-Gordon, M. *J. Chem. Phys.* **2009**, *131*, 174105.
(56) Runge, E.; Gross, E. K. U. *Phys. Rev. Lett.* **1984**, *52*, 997.
(57) Casida, M. E. *Time-dependent density functional response theory for molecules*; World Scientific: Singapore, 1995.
(58) Fedorov, D. G.; Kitaura, K. *The Fragment Molecular Orbital Method: Practical Applications to Large Molecular Systems*; CRC Press: Boca Raton, FL, 2009.
(59) Kitaura, K.; Ikeo, E.; Asada, T.; Nakano, T.; Uebayasi, M. *Chem. Phys. Lett.* **1999**, *313*, 701.
(60) Moller, C.; Plesset, M. S. *Phys. Rev.* **1934**, *46*, 618.
(61) Chen, W.; Gordon, M. S. *J. Phys. Chem.* **1996**, *100*, 14316.
(62) Fedorov, D. G.; Slipchenko, L. V.; Kitaura, K. *J. Phys. Chem. A* **2010**, *114*, 8742.
(63) Kitaura, K.; Morokuma, K. *Int. J. Quantum Chem.* **1976**, *10*, 325.
(64) Ghosh, D.; Kosenkov, D.; Vanovschi, V.; Williams, C. F.; Herbert, J. M.; Gordon, M. S.; Schmidt, M. W.; Slipchenko, L. V.; Krylov, A. I. *J. Phys. Chem. A* **2010**, *114*, 12739.
(65) Gordon, M. S.; Slipchenko, L. V.; Li, H.; Jensen, J. H. *Annu. Rep. Comput. Chem.* **2007**, *3*, 177.
(66) Reed, A. E.; Curtiss, L. A.; Weinhold, F. *Chem. Rev.* **1988**, *88*, 899.
(67) Yang, J. H.; Christianson, L. A.; Gellman, S. H. *Org. Lett.* **1999**, *1*, 11.
(68) Cisneros, G. A.; Tholander, S. N. I.; Parisel, O.; Darden, T. A.; Elking, D.; Perera, L.; Piquemal, J. P. *Int. J. Quantum Chem.* **2008**, *108*, 1905.
(69) Elking, D. M.; Cisneros, G. A.; Piquemal, J. P.; Darden, T. A.; Pedersen, L. G. *J. Chem. Theory Comput.* **2010**, *6*, 190.
(70) Pilme, J.; Piquemal, J. P. *J. Comput. Chem.* **2008**, *29*, 1440.
(71) Ponder, J. W.; Wu, C.; Ren, P.; Pande, V. S.; Chodera, J. D.; Schnieders, M. J.; Haque, I.; Mobley, D. L.; Lambrecht, D. S.; DiStasio, R. A.; Head-Gordon, M.; Clark, G. N. I.; Johnson, M. E.; Head-Gordon, T. *J. Phys. Chem. B* **2010**, *114*, 2549.
(72) Chass, G. A.; Mirasol, R. S.; Setiadi, D. H.; Tang, T. H.; Chin, W.; Mons, M.; Dimicoli, I.; Dognon, J. P.; Viskolcz, B.; Lovas, S.; Penke, B.; Csizmadia, I. G. *J. Phys. Chem. A* **2005**, *109*, 5289.
(73) Stanca-Kaposta, E. C.; Gamblin, D. P.; Cocinero, E. J.; Frey, J.; Kroemer, R. T.; Fairbanks, A. J.; Davis, B. G.; Simons, J. P. *J. Am. Chem. Soc.* **2008**, *130*, 10691.
(74) Brause, R.; Fricke, H.; Gerhards, M.; Weinkauf, R.; Kleinermanns, K. *Chem. Phys.* **2006**, *327*, 43.
(75) Reed, A. E.; Weinhold, F. *J. Chem. Phys.* **1985**, *83*, 1736.
(76) Chin, W.; Mons, M.; Dognon, J. P.; Mirasol, R.; Chass, G.; Dimicoli, I.; Piuzzi, F.; Butz, P.; Tardivel, B.; Compagnon, I.; von Helden, G.; Meijer, G. *J. Phys. Chem. A* **2005**, *109*, 5281.
(77) Bader, R. F. W. *J. Phys. Chem. A* **2009**, *113*, 10391.
(78) Bader, R. F. W. *J. Phys. Chem. A* **2010**, *114*, 7431.
(79) Rizzo, T. R.; Stearns, J. A.; Boyarkin, O. V. *Int. Rev. Phys. Chem.* **2009**, *28*, 481.